
SRSR: Enhancing Semantic Accuracy in Real-World Image Super-Resolution with Spatially Re-Focused Text-Conditioning

Chen Chen^{1,2*} Majid Abdolshah¹ Violetta Shevchenko¹
 Hongdong Li^{1,3} Chang Xu² Pulak Purkait¹
¹Amazon ²The University of Sydney ³Australian National University

Abstract

Existing diffusion-based super-resolution approaches often exhibit semantic ambiguities due to inaccuracies and incompleteness in their text conditioning, coupled with the inherent tendency for cross-attention to divert towards irrelevant pixels. These limitations can lead to semantic misalignment and hallucinated details in the generated high-resolution outputs. To address these, we propose a novel, plug-and-play *spatially re-focused super-resolution (SRSR)* framework that consists of two core components: first, we introduce Spatially Re-focused Cross-Attention (SRCA), which refines text conditioning at inference time by applying visually-grounded segmentation masks to guide cross-attention. Second, we introduce a Spatially Targeted Classifier-Free Guidance (STCFG) mechanism that selectively bypasses text influences on ungrounded pixels to prevent hallucinations. Extensive experiments on both synthetic and real-world datasets demonstrate that SRSR consistently outperforms seven state-of-the-art baselines in standard fidelity metrics (PSNR and SSIM) across all datasets, and in perceptual quality measures (LPIPS and DISTs) on two real-world benchmarks, underscoring its effectiveness in achieving both high semantic fidelity and perceptual quality in super-resolution.

1 Introduction

Image super-resolution (SR) aims to restore a high-resolution (HR) image from a low-resolution (LR) counterpart degraded by blur, noise, and compression artifacts or other distortions. This classic problem has broad real-world applications, ranging from photography [18] and digital surveillance [63, 32] to medical imaging [12, 41, 17] and remote sensing [45]. However, restoring both photorealistic details and semantically coherent content under severe degradations remains an open challenge. Early deep-learning-based approaches often assume simple, known degradations (e.g., bicubic or Gaussian downsampling) and investigate new architectural designs [3, 4, 8, 9, 24, 28, 38, 67]. Subsequently, super-resolution methods based on generative models like GANs [11] and diffusion models [16, 29] can produce realistic details [62, 46, 19, 49], yet they frequently struggle on real-world LR image inputs that deviate from the above assumptions, resulting in clear artifacts in the super-resolved outputs. Consequently, recent research adopts more complex and realistic degradation pipelines (e.g., Real-ESRGAN [46]) and exploits the powerful Stable Diffusion (SD) prior [36], as in StableSR [44] and DiffBIR [25], to improve generalization in real-world ISR. However, these methods overlook textual guidance, thus risking semantic misalignment.

A recent trend is to incorporate text priors to guide super-resolution via a text-to-image Stable Diffusion pipeline, leading to better semantic fidelity [58, 59, 31, 54, 53]. Among these methods, the degradation-aware prompt extractor (DAPE) proposed by SeeSR [54] demonstrates superior

*Work done during internship at Amazon.

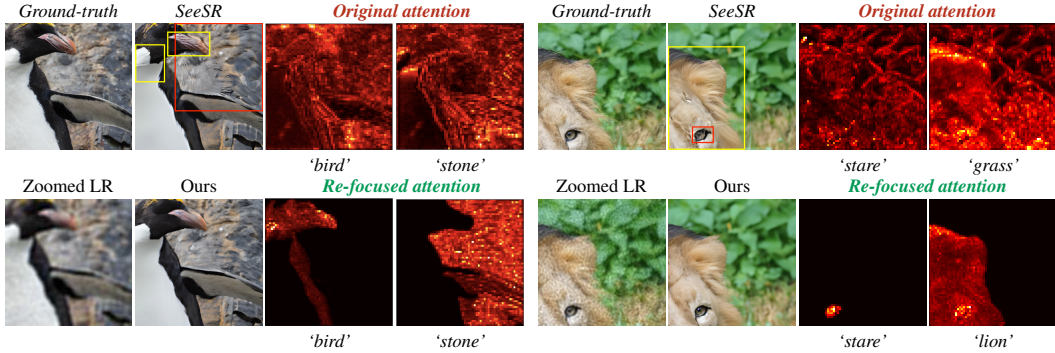


Figure 1: Illustrations of how inherent cross-attention can be misled by irrelevant tokens, resulting in semantically incorrect restorations (top). Left: the baseline mistakenly associates the stone region with the token ‘bird’, and the animal’s neck and beak with ‘stone’, producing wing-like artifacts on the stone and unnatural textures on the animal. Right: attention for ‘stare’ is scattered across irrelevant patches, and both the eye and lion face incorrectly respond to ‘grass’, introducing hallucinated textures. We propose re-focusing cross-attention by constraining the influence of each text token to its grounded region, yielding sharper and semantically aligned reconstructions (bottom).

performance in terms of both degradation-awareness and efficiency compared to other off-the-shelf models used like ResNet [14], YOLO [33], BLIP [23] and LLaVA [26] employed in other works. OSediff [53] further trains a one-step model that also leverages DAPE as the prompt extractor.

Despite these advances, text conditioning can induce hallucinations, causing ambiguous semantics in the restored results, as illustrated in Fig. 1. We identify three main limitations in current designs: *Firstly*, existing approaches rely exclusively on cross-attention to inject text prompts, but tokens often leak onto unrelated regions, leading to mismatched guidance and semantic ambiguity. *Secondly*, although DAPE is more degradation-aware than other prompt extractors, it remains only partially robust to severe degradations, making accurate prompt extraction challenging. Providing erroneous text prompts can degrade the fidelity of super-resolved outputs more severely than omitting text guidance altogether. *Thirdly*, prompt extraction methods do not guarantee full-image coverage, leaving ungrounded regions without guidance from relevant semantics and vulnerable to the influence of unrelated text prompts. A recent work [40] exploits Mask2Former [5] trained on ADE20K [70] to achieve full-image coverage by assigning dense segmentation labels to every pixel. However, its segmentation model lacks degradation-awareness and is restricted to 150 categories, limiting its scope for real-world applications that demand open-vocabulary understanding. Bridging these limitations to achieve fully coherent, semantically correct super-resolution remains an open challenge.

To address the aforementioned challenges, we propose a novel framework that conducts *Spatially Re-focused Super-Resolution (SRSR)*. We first apply *visual grounding* to filter out less relevant tags and generate tag-region pairs via segmentation masks. Based on these, we introduce *Spatially Re-focused Cross-Attention (SRCA)*, which constrains each tag’s influence to its corresponding spatial region, effectively mitigating semantic hallucinations from the first two limitations. To further improve restoration in ungrounded regions, we introduce a *Spatially Targeted Classifier-Free Guidance (STCFG)* mechanism that selectively disables classifier-free guidance in these regions to avoid undesired text-conditioning effects. Notably, our method operates exclusively at inference time, eliminating the need for additional training or fine-tuning. As a result, it serves as a lightweight, plug-and-play module compatible with any cross-attention-based SR approach that utilizes text priors.

Our results show that incorporating SRSR into both the 1-step OSediff and the 50-step SeeSR baselines yields significant improvements in full-reference metrics across synthetic and real-world datasets. When compared to seven other state-of-the-art baselines, our method consistently outperforms all alternatives in fidelity measures PSNR and SSIM on every dataset, and achieves the top performance for perceptual metrics LPIPS and DISTS on the two real-world datasets (RealSR and DrealSR) while ranking second on the synthetic DIV2K set. In summary, our contributions are threefold: *First*, we highlight underexplored gaps in existing methods that impede semantically accurate super-resolution. *Second*, we propose a novel SRSR framework that effectively alleviates semantic ambiguity through spatially re-focused cross-attention (SRCA) and spatially targeted CFG (STCFG), while remaining a lightweight, inference-time plug-and-play module for any cross-attention-based SR approach with text priors. *Third*, SRSR achieves new state-of-the-art performance against seven strong baselines.

2 Related work

2.1 Non-diffusion-based super-resolution methods

Starting with CNN-based approaches, SR has been extensively explored through models that directly map LR images to HR outputs in an end-to-end manner [21, 69, 13, 9, 39, 6]. Many CNN-based methods focus on designing deeper or wider networks and improving attention mechanisms to enhance SR performance [48]. With the rise of generative models, GANs have gained popularity by using adversarial frameworks where the generator creates HR images closely matching real image distributions, thereby improving perceptual quality and realism. Real-ESRGAN [46] advanced this by introducing a high-order degradation model and modifying the U-Net discriminator to enhance stability and visual performance in real-world SR scenarios. Building on this, uncertainty and semantic-aware approaches have been proposed [27, 42, 22, 61, 30]. Uncertainty-Aware GANs [27] integrated pixel-level uncertainty into adversarial training for fine-grained feedback, while SeD [22] incorporated semantic information into the discriminator to guide the generator in producing semantically aligned textures. CAL-GAN [61], another context-aware method, employs a mixture of classifiers to handle image patches based on content, improving discriminator capacity for photo-realistic SR. In parallel, SFT-GAN [47] demonstrates how spatially-varying categorical priors derived from semantic segmentation maps can be integrated into SR networks through Spatial Feature Transform (SFT) layers, enabling region-specific modulation of features and the recovery of textures that are more realistic and faithful to underlying semantics. However, these methods primarily focus on broader image-level semantic context rather than explicitly leveraging object-level understanding within images for SR.

2.2 Diffusion-based super-resolution methods

DDRM and DDNM [19, 49] were the earlier efforts that develop DDPM-based SR methods. Subsequently, Stable-Diffusion-based SR methods like StableSR [44] and DiffBIR [25] were proposed to tackle the more challenging real-world image super-resolution (Real-ISR) task by leveraging Stable Diffusion (SD)’s strong prior that trained using billions of image-text pairs. A recent trend is to incorporate text priors to guide generation in text-to-image SD, leading to better semantic fidelity. For example, CoSeR [37] highlights the potential of bridging image and language understanding using diffusion-based priors and cognitive embeddings. Also, PASD [58] extracts text prompts via off-the-shelf models (ResNet [14], YOLO [33] and BLIP [23]) and leverages ControlNet [65] without modifying SD’s pre-trained weights. SUPIR [59] and XPSR [31] employ LLaVA [26], while SeeSR [54] proposes a degradation-aware prompt extractor (DAPE) that improves on the Recognize Anything Model (RAM) [68] for LR images. OSEDiff [53] further trains a one-step model that also leverages DAPE as the prompt extractor, demonstrating its superiority over larger vision-language models like LLaVA. Most recent works like SegSR [55] and HolisDiP [40] propose to additionally use semantic segmentation models to extract prompts with more comprehensive coverage. Despite these advances, ensuring the accuracy of the extracted prompt and the robustness of its cross-attention injection remains difficult under heavy degradation, as incorrect text guidance can still trigger hallucinations and semantic ambiguity in the restored outputs.

3 Method

3.1 Research gaps

Recent work has shown that super-resolution (SR) methods based on Stable Diffusion (SD) hold promise, primarily due to SD’s powerful prior learned from billions of image-text pairs. However, when operating on degraded LR images, semantic errors can arise, leading to inaccurate reconstructions. Recent studies [58, 54, 59, 53] have demonstrated that leveraging SD’s text-conditioning, guided by text priors extracted from LR images, can yield more semantically-aware SR results. Nevertheless, hallucination is often observed due to three major limitations of the current designs:

Diverted cross-attention. Existing approaches rely on cross-attention to implicitly associate text prompts with image pixels. However, we observe that these associations are often misaligned, with text tokens attending to irrelevant regions. As shown in Fig. 1 (top row), the baseline cross-attention maps frequently misattribute tokens such as ‘bird’, ‘stone’, ‘stare’, and ‘grass’ to unrelated image areas, leading to semantic ambiguity and perceptual artifacts. The output’s semantic fidelity is further degraded when the extracted text contains incorrect or loosely related tags. For instance, in Fig. 2 (top row), ‘tower’ is loosely relevant to ‘building’, but the latter is mainly used for guiding the restoration of the building regions. In contrast, ‘tower’ pays significant attention to regions highlighted by the yellow bounding boxes, which actually correspond to tree-like structures, introducing hallucinated

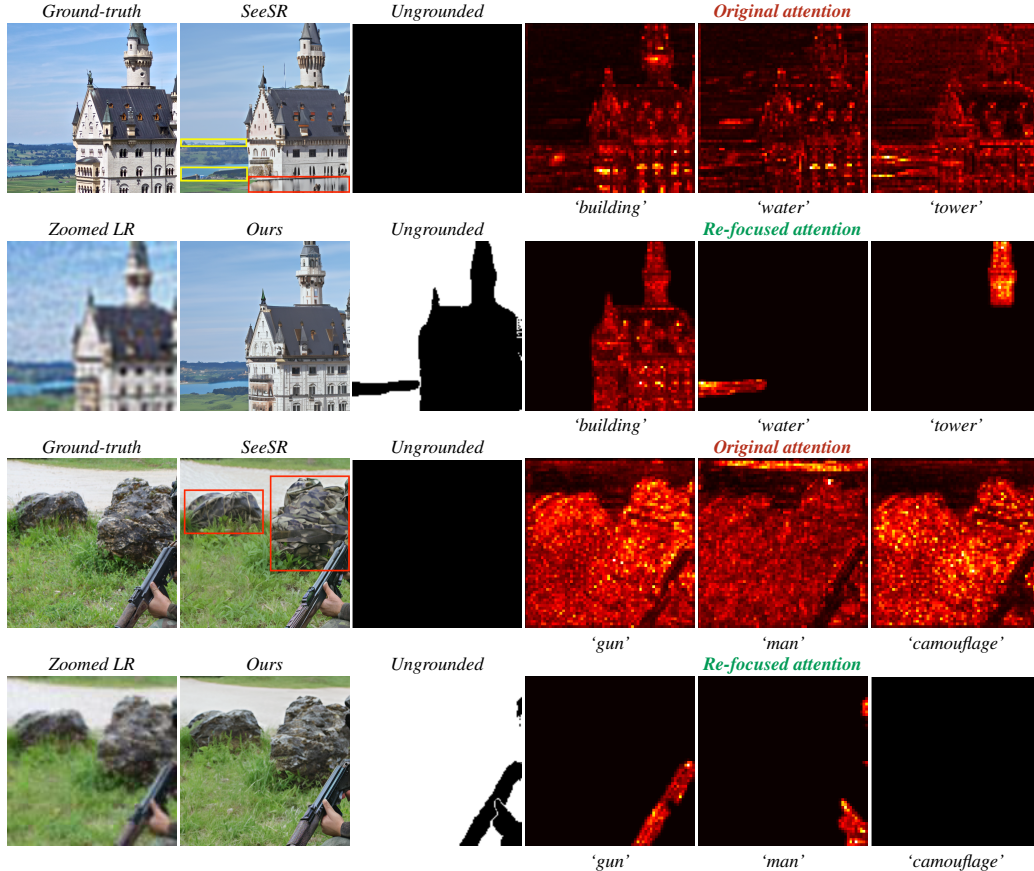


Figure 2: Analysis of how our proposed *Spatially Re-focused Cross-Attention (SRCA)* and *Spatially Targeted Classifier-Free Guidance (STCFG)* improve semantic fidelity in text-conditioned super-resolution. The *Ungrounded* mask highlights regions where no textual tag can be confidently grounded. Existing methods rely solely on inherent cross-attention, allowing global or irrelevant tokens to influence all regions. *SRCA* addresses this by limiting each token’s influence to its corresponding grounded region only, reducing semantic confusion. However, this leaves ungrounded regions only associated with global tokens (e.g., EOS, padding, punctuation), where summary tokens like EOS can still carry semantics of the entire prompt and influence its restoration. To resolve this, *STCFG* disables text conditioning entirely in ungrounded areas by using unconditional noise prediction in the reverse diffusion process, further enhancing the ungrounded region’s restoration.

content where it does not belong. A similar issue is shown in Fig. 2 (third row), where the incorrect tag ‘camouflage’ is extracted by DAPE from the degraded LR image. As a result, the SeeSR baseline synthesizes camouflage-like patterns in regions (highlighted in red boxes) that should depict stones. Although the output appears visually plausible, it suffers from poor semantic fidelity.

Incorrect prompts. Extracting accurate text prompts from LR images remains challenging. Recent efforts, such as the degradation-aware prompt extractor (DAPE) [54], improve on the Recognize Anything Model (RAM) but still produce misleading prompts under severe degradation. Injecting these incorrect signals can lead to even more erroneous SR results than using no text guidance at all.

Incomplete prompts. While DAPE demonstrates greater robustness to image degradations than many alternative text extractors, it does not guarantee comprehensive coverage of the entire image. It may miss salient objects and often fails to assign tags to non-object background regions due to its object-centric design. As a result, uncovered regions encounter two key issues: (1) they lack the semantic guidance that tagged regions benefit from, and (2) they remain susceptible to influence from unrelated text prompts, leading to hallucinations in areas that should remain unaffected.

In response, we propose a novel *Spatially Re-focused Super-Resolution (SRSR)* framework (Fig. 3) that comprises two key components. First, the *Spatially Re-focused Cross-Attention (SRCA)* module (Sec. 3.2) tackles the first two gaps by mitigating semantic ambiguity and reducing the influence of

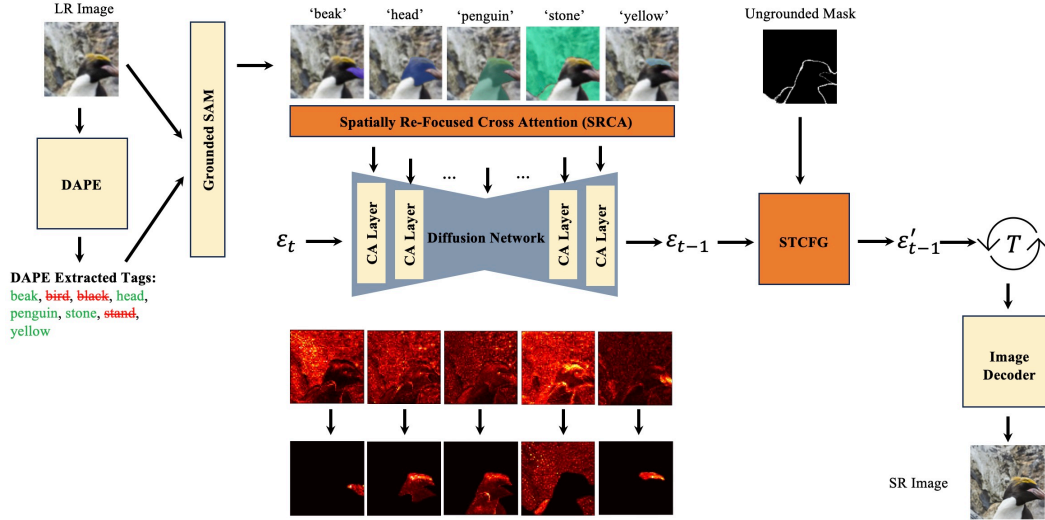


Figure 3: Overview of our proposed pipeline. First, the LR image is processed by a Degradation-Aware Prompt Extractor (DAPE) [54] to obtain text tags. Both the LR image and the extracted tags are then passed to Grounded SAM, which produces visually grounded tag–mask pairs. We also define an ungrounded mask as the complement of the union of all grounded masks. Next, each tag–mask pair is integrated into all 16 U-Net cross-attention layers, using the masks to constrain text conditioning precisely to relevant regions. Once noise prediction is complete, we selectively apply Classifier-Free Guidance (CFG) to grounded pixels while leaving ungrounded pixels under unconditional guidance, ensuring they remain unaffected by the text prompts. After T denoising steps, a final decoder maps the latent representation back to pixel space, yielding the super-resolved (SR) image.

incorrect or loosely related tags through spatially constrained attention. Second, the *Spatially Targeted Classifier-Free Guidance (STCFG)* module (Sec. 3.3) targets the third limitation by improving restoration in regions lacking explicit grounding. Notably, SRSR is designed as an efficient, inference-only solution that requires no additional training or fine-tuning, making it compatible as a plug-and-play module with any cross-attention-based super-resolution method that utilizes text priors.

3.2 Spatially Re-focused Cross-Attention (SRCA)

First, we ground the DAPE-extracted tags onto the image using Grounded SAM [35], assigning each tag to a specific region. This step offers two key benefits: (1) tags that cannot be confidently grounded are likely irrelevant and thus removed, avoiding the injection of erroneous signals into the super-resolution process, addressing the aforementioned second limitation; (2) each grounded tag is now accompanied by a segmentation mask, enabling our proposed *Spatially Re-focused Cross-Attention (SRCA)* mechanism to mitigate semantic ambiguity and address the aforementioned first limitation.

With these text-mask pairs, SRCA refines the spatial precision of text conditioning, effectively reducing semantic ambiguity in the super-resolved outputs. Specifically, instead of only relying on the implicit cross-attention itself, we explicitly leverage each tag’s corresponding segmentation mask to localize and re-focus the attention of text-conditioning, effectively suppressing attention outside the designated target regions. This ensures that each text token attends exclusively to its intended image regions, mitigating distractions from irrelevant areas. See Fig. 1 and 2 for visual analysis.

Formally, the cross-attention mechanism computes attention weights α_{ij} for pixel i and token j as:

$$\alpha_{ij} = \text{SoftMax}\left(\frac{Q_i \cdot K_j}{\sqrt{d}}\right), \quad (1)$$

where Q and K are query and key embeddings, respectively, and d is the feature dimension. These weights form a weighted sum of the token values V_j to obtain O_i , which is the output for pixel i :

$$O_i = \sum_j \alpha_{ij} V_j, \quad (2)$$

In SRCA, we first apply a binary mask M_{ij} (1 for valid regions) to refine the attention weights α_{ij} :

$$\alpha_{ij}^{\text{SRCA}} = M_{ij} \alpha_{ij}. \quad (3)$$

We then re-normalize these masked weights across both pixel and token dimensions:

$$\hat{\alpha}_{ij}^{\text{SRCA}} = \frac{\alpha_{ij}^{\text{SRCA}}}{\sum_{i',j'} \alpha_{i'j'}^{\text{SRCA}}}. \quad (4)$$

This preserves proper attention distribution and ensures that zeroed-out entries do not distort the attention map while preserving the normalization of valid tokens, ensuring they continue to sum to one. As a result, this re-focusing operation suppresses contributions from irrelevant tokens, ensuring that each pixel i attends only to the relevant tokens while maintaining consistent overall attention magnitudes. For example, for pixel i , a relevant token V_m would correspond to $M_{im} = 1$, resulting in the attention weight unchanged $\alpha_{ij}^{\text{SRCA}} = \alpha_{ij}$. Conversely, for an irrelevant token V_n , the segmentation mask would have $M_{in} = 0$, resulting in no attention is placed on such a token. Importantly, as Eq. 2 computes weighted average of all tokens, eliminating such irrelevant token also helps increase the attentions to the relevant tokens. Consequently, SRCA produces more contextually aligned super-resolution results, with enhanced focus on the key regions of the image.

3.3 Spatially Targeted CFG application (STCFG)

Although our proposed SRCA in Sec. 3.2 addresses the first two limitations, the third limitation of insufficient tag coverage remains. Moreover, when our grounding mechanism is overly conservative and discards tags that are partially relevant, coverage can be reduced further. Resolving this issue is crucial for improving our overall performance. A recent work [40] proposed an interesting approach to address this challenge by employing Mask2Former [5], trained on ADE20K [70], to generate semantic segmentation labels for each image region, which are then used as text conditions. However, unlike DAPE, Mask2Former is not degradation-aware and often produces inaccurate labels when applied to degraded LR images, failing to resolve the second limitation and ultimately resulting in inferior performance. Furthermore, the model trained on ADE20K is limited to a fixed set of 150 categories, which restricts its expressiveness and precision in practice. Through additional ablation studies (Tab. 2), we observe that using these additional segmentation tags in the prompt leads to degraded performance. We also tested open-vocabulary segmentation methods, such as Prompt-Free Anything Detection and Segmentation in DINO-X [34], and observed that while they outperformed Mask2Former, their lack of degradation-awareness similarly led to inaccurate tags and inferior results compared to using DAPE alone. These indicate that inaccuracies are more harmful than incomplete coverage for text conditionings. More discussions are available in the ablation studies (Sec. 4.3).

Given the inherent difficulty and threshold sensitivity in balancing accuracy and coverage of tags extracted from degraded LR images, we note that the coverage limitation affects only the ungrounded regions. Instead of fine-tuning thresholds, can we explore an alternative that directly improves ungrounded-region quality by design without risking incorrect prompts? Drawing from our insight that erroneous tags are more detrimental than no tags, we argue that omitting guidance is preferable to providing incorrect conditioning. In standard CFG, a text-conditional output $\epsilon_{\theta}(x_t, y)$ is balanced against an unconditional output $\epsilon_{\theta}(x_t, \phi)$. The combined prediction $\hat{\epsilon}$ is typically computed as:

$$\hat{\epsilon} \leftarrow \epsilon_{\theta}(x_t, \phi) + s[\epsilon_{\theta}(x_t, y) - \epsilon_{\theta}(x_t, \phi)], \quad (5)$$

where $s \geq 1$ is the guidance scale, indicating a positive weight is applied to the text-conditional generation, while a non-positive weight is assigned to the unconditional generation. However, uniformly applying CFG can degrade ungrounded regions because they only receive prompts from semantic-free or summary global tokens (e.g., EOS, padding, punctuation), where summary tokens like EOS can still carry semantics of the entire prompt and influence its restoration. To address this, we construct an ungrounded mask M for each image by taking the complement of the union of all grounded segmentation masks (i.e., $M = 1$ for ungrounded pixels and 0 for grounded pixels). We then *selectively* apply CFG only to grounded pixels, while leaving the ungrounded pixels unconditional:

$$\hat{\epsilon}_i \leftarrow (1 - M_i) \left[\epsilon_{\theta}(x_t, \phi) + s(\epsilon_{\theta}(x_t, y) - \epsilon_{\theta}(x_t, \phi)) \right] + M_i \epsilon_{\theta}(x_t, \phi), \quad (6)$$

where $M_i \in \{0, 1\}$ indicates whether pixel i is ungrounded. This targeted approach ensures that uncertain or irrelevant tags do not influence the restoration of ungrounded regions, while grounded pixels still benefit from text conditioning, thereby preserving the visual fidelity.

Table 1: Quantitative comparison with state-of-the-art methods on both synthetic and real-world baselines. ‘s’ denotes the number of diffusion reverse steps. **Red** = best, **Blue** = second-best.

Dataset	Method	Metric								
		PSNR \uparrow	SSIM \uparrow	LPIPS \downarrow	DISTS \downarrow	FID \downarrow	NIQE \downarrow	MUSIQ \uparrow	MANIQA \uparrow	CLIPIQ \uparrow
RealSR	StableSR-s200	24.70	0.7085	0.3018	0.2288	128.51	5.9122	65.78	0.6221	0.6178
	DiffBIR-s50	24.75	0.6567	0.3636	0.2312	128.99	5.5346	64.98	0.6246	0.6463
	PASD-s20	25.21	0.6798	0.3380	0.2260	124.29	5.4137	68.75	0.6487	0.6620
	ResShift-s15	26.31	0.7421	0.3460	0.2498	135.93	7.2635	58.43	0.5285	0.5444
	SinSR-s1	26.28	0.7347	0.3188	0.2353	131.93	6.2872	60.80	0.5385	0.6122
	OSDiff-s1	24.43	0.7153	0.3173	0.2363	125.97	6.3897	67.52	0.6168	0.6742
	SeeSR-s50	25.18	0.7216	0.3009	0.2223	125.55	5.4081	69.77	0.6442	0.6612
	SRSR-OSDiff-s1	24.53	0.7206	0.3166	0.2378	132.55	6.6106	67.24	0.6137	0.6710
	SRSR-SeeSR-s50	26.40	0.7632	0.2718	0.2092	126.31	5.8627	62.88	0.5628	0.5409
	DIV2K-Val	StableSR-s200	23.26	0.5726	0.3113	0.2048	24.44	4.7581	65.92	0.6192
DiffBIR-s50		23.64	0.5647	0.3524	0.2128	30.72	4.7042	65.81	0.6210	0.6704
PASD-s20		23.14	0.5505	0.3571	0.2207	29.20	4.3617	68.95	0.6483	0.6788
ResShift-s15		24.65	0.6181	0.3349	0.2213	36.11	6.8212	61.09	0.5454	0.6071
SinSR-s1		24.41	0.6018	0.3240	0.2066	35.57	6.0159	62.82	0.5386	0.6471
OSDiff-s1		23.31	0.5970	0.3046	0.2129	26.80	5.4031	65.56	0.5857	0.6588
SeeSR-s50		23.68	0.6043	0.3194	0.1968	25.90	4.8102	68.67	0.6240	0.6936
SRSR-OSDiff-s1		23.43	0.6023	0.3053	0.2142	27.65	5.5389	65.08	0.5797	0.6531
SRSR-SeeSR-s50		24.72	0.6416	0.3275	0.1991	25.31	5.4986	59.55	0.5402	0.5518
DRealSR		StableSR-s200	28.03	0.7536	0.3284	0.2269	148.98	6.5239	58.51	0.5601
	DiffBIR-s50	26.71	0.6571	0.4557	0.2748	166.79	6.3124	61.07	0.5930	0.6395
	PASD-s20	27.36	0.7073	0.3760	0.2531	156.13	5.5474	64.87	0.6169	0.6808
	ResShift-s15	28.46	0.7673	0.4006	0.2656	172.26	8.1249	50.60	0.4586	0.5342
	SinSR-s1	28.36	0.7515	0.3665	0.2685	170.57	6.9907	55.33	0.4884	0.6383
	OSDiff-s1	27.65	0.7743	0.3177	0.2366	141.96	7.3050	63.55	0.5758	0.7060
	SeeSR-s50	28.17	0.7691	0.3189	0.2315	147.39	6.3967	64.93	0.6042	0.6804
	SRSR-OSDiff-s1	27.72	0.7781	0.3178	0.2379	139.66	7.5271	63.62	0.5736	0.7010
	SRSR-SeeSR-s50	29.50	0.8128	0.2866	0.2176	146.98	7.1279	54.04	0.4962	0.5513

Visually, as shown in Fig. 2, SRCA and STCFG play complementary roles. SRCA improves the semantic fidelity of grounded objects by refining the cross-attention maps. In the top example, the SeeSR baseline mistakenly restores part of the building (highlighted in red) as water-like due to attention leakage from the ‘water’ token. SRCA re-focuses the attention of both ‘building’ and ‘water’ tokens to their correct regions, leading to the accurate restoration of the entire building. However, SRCA falls short in suppressing the influence of global tokens on ungrounded regions (as visualized by the ungrounded masks). To address this, STCFG applies unconditional guidance to those regions, effectively preventing hallucinations and yielding more faithful restorations, as qualitatively observed.

4 Experimental results

4.1 Setup

Datasets. Unlike prior approaches [44, 25, 58, 54, 53] that require training, our proposed SRSR operates purely at inference time and therefore only needs test datasets. Following the baselines, we adopt the standard test set from StableSR [44], which includes both synthetic and real-world data. The synthetic portion contains 3,000 images (512×512), whose ground truths (GT) are randomly cropped from DIV2K-Val [1] and degraded via the Real-ESRGAN pipeline [46]. The real-world portion comprises LQ-HQ pairs from RealSR [2] (128×128) and DRealSR [52] (512×512), respectively.

Baseline methods. SRSR is a plug-and-play module that integrates seamlessly into any cross-attention-based SR approach utilizing text priors, offering performance gains without additional training. To validate its effectiveness, we incorporate SRSR into two state-of-the-art methods: a 50-step method, SeeSR [54], and a single-step method, OSDiff [53]. Users can select between these baselines based on their preferred trade-off between efficiency and quality, since multi-step approaches often yield better results at the expense of increased computation.

We further compare our SRSR-SeeSR and SRSR-OSDiff variants against a range of strong baselines under their standard configurations, including StableSR [44], DiffBIR [25], PASD [58], ResShift [60], and SinSR [50]. Among these, ResShift trains a diffusion model from scratch in the pixel space, while SinSR is a one-step distilled model derived from ResShift. The remaining methods operate in latent space and build on top of the pre-trained SD model.

Evaluation metrics. In line with prior work, we evaluate using both full-reference and no-reference metrics. For full-reference evaluation, we use PSNR and SSIM [51] as fidelity measures, and LPIPS [66] and DISTS [7] to assess perceptual quality. FID [15] is also employed to gauge the distributional distance between super-resolved and ground-truth high-resolution (HR) images. For no-reference assessment, we adopt NIQE [64], MANIQA-pipal [57], MUSIQ [20], and CLIPQA [43].

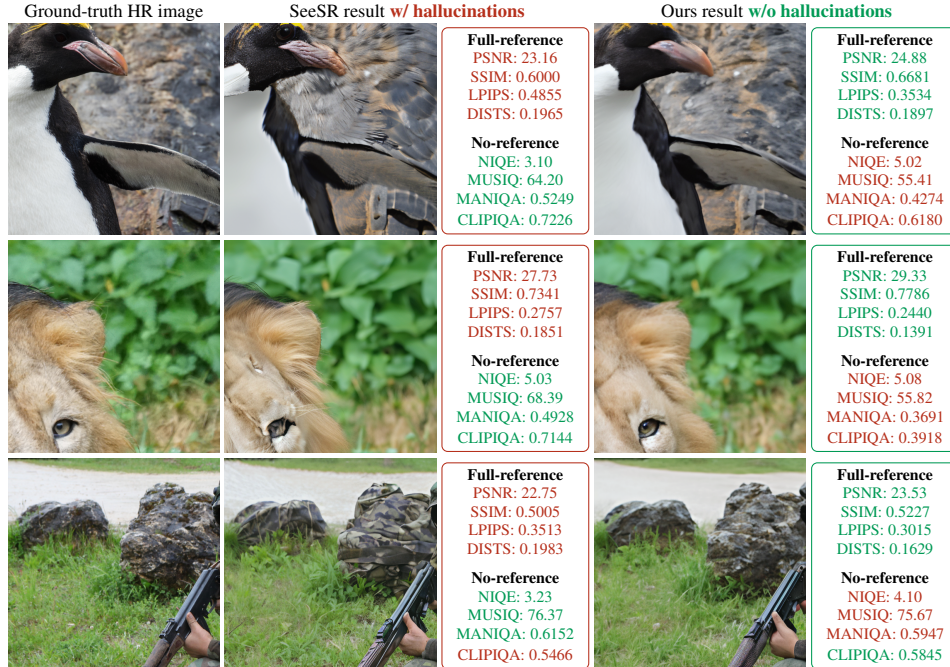


Figure 4: Qualitative results show that the baseline method exhibits clear semantic hallucinations. In contrast, plugging SRSR into the baseline leads to semantically faithful restorations. All full-reference metrics, including both fidelity (PSNR and SSIM) and perceptual quality (LPIPS and DIST) measures, consistently validate the improvements brought by our method. However, it is worth noting that *the no-reference metrics tend to misjudge and heavily reward hallucinated results* due to their design, as indicated by the significant performance gap observed despite degraded semantic realism. This exposes their limitations in assessing semantic fidelity for super-resolution.

Implementation details. We adopt DAPE [54] as our prompt extractor, following its use in both SeeSR and OSEDiff. DAPE excels at handling degraded LR images while being more efficient than advanced multimodal vision-language models [26]. Although we experimented with various semantic segmentation models (e.g., Mask2Former [5] and Prompt-Free Anything Detection/Segmentation in DINO-X [34]), they did not make it into our final SRSR design. For grounding, we employ Grounded SAM 2, which is a combined framework built upon DINO-X and SAM 2.

Complexity analysis. Within our proposed SRSR framework, both SRCA and STCFG are applied only during inference and modify the cross-attention and CFG processes dynamically without introducing any new learnable parameters. Our approach uses the same pretrained diffusion model and UNet architecture as the baseline, so the parameter count remains the same. Therefore, the performance gains are achieved without increasing model complexity or adding new parameters.

Efficiency analysis. Our integration of Grounded SAM into the pipeline is highly efficient. *First*, it requires only a single inference per image before the SR process to pre-compute the masks, using the low-resolution (LR) input. The resulting masks are cached and reused during inference, avoiding repeated computation. *Second*, since only the LR image (e.g., 128×128) is fed into Grounded SAM, the processing time is minimal (just 0.12s per image) on V100, and even for 512×512 inputs, it remains low at 0.16s, making our approach practical and scalable for real-world applications. This pre-processing step also does not affect the parameter count or inference complexity.

4.2 Comparisons with state-of-the-art baselines

Tab. 1 compares our methods against several state-of-the-art baselines. To highlight SRSR’s contribution, note how it improves a given baseline: for instance, applying SRSR to SeeSR considerably boosts full-reference fidelity measures PSNR and SSIM across all three datasets. It also enhances the full-reference perceptual quality metrics LPIPS and DIST on two real-world sets (RealSR and DRealSR) while offering comparable performance on synthetic data (DIV2K-Val). No-reference metrics, however, often favor strong semantic cues, even if they are inaccurate, where it is frequently observed that hallucinated restorations have high performance in no-reference metrics, making them less reliable. Examples can be observed from Fig. 4. We also evaluate SRSR on OSEDiff,

which differs from SeeSR in two key aspects: it is a one-step inference method (confirming SRSR’s flexibility regarding inference steps) and does not employ classifier-free guidance (CFG) (making STCFG inapplicable). In this setting, only the SRCA module is integrated. Despite this, we observe consistent improvements in fidelity metrics (PSNR and SSIM) across all datasets, with only marginal trade-offs in perceptual quality (LPIPS and DISTS), demonstrating SRCA’s standalone effectiveness in enhancing semantic accuracy. This observation is further supported by the comparison between V2 and V3 in Tab. 2, which highlights the standalone effectiveness of SRCA without STCFG. The slight drop in perceptual quality arises from ungrounded regions still receiving text-conditioning from summary or meaningless tokens (e.g., EOS, punctuation), which STCFG is designed to address. This indicates that while SRSR is broadly compatible with diverse frameworks, its full potential is best realized when the underlying method supports CFG. Nonetheless, using SRCA alone is valuable in common scenarios where semantic fidelity is prioritized over background perceptual quality. These results highlight SRCA’s independent benefits and STCFG’s complementary role.

Beyond direct baselines, we have also compare with a range of strong competitors, where our methods generally achieve the best performance on full-reference fidelity and perceptual metrics, falling short of the top rank only in LPIPS and DISTS on DIV2K-Val, yet still securing second place in such cases.

4.3 Ablation studies

Grounding. As discussed in Sec. 3.2 and Sec. 3.3, grounding increases tag accuracy by discarding irrelevant text at the expense of reduced coverage when certain relevant tags are mistakenly removed. This reflects an accuracy-completeness trade-off in tag extraction. Experimentally, we find that accuracy typically outweighs completeness: providing fewer but more relevant tags produces better results than including extra but less reliable ones. For instance, comparing V1 and V2 in Tab. 2 shows that simply applying grounding (V2) to the SeeSR baseline yields small gains in three out of four metrics. Moreover, V5 differs from our final V4 only by including ungrounded tags, which lowers performance on all four metrics. Additionally, grounding’s effectiveness depends on its confidence threshold, which balances strictness (accuracy) against coverage (completeness). We further explore this trade-off in Sec. 4.4. Finally, it is also worth emphasizing that grounding does more than just manage the accuracy-completeness trade-off: it also enables spatial re-focusing through SRCA, whereby each grounded tag is paired with a segmentation mask to alleviate semantic ambiguity.

Spatially Re-focused Cross-Attention (SRCA). SRCA mitigates semantic ambiguities and enhances output fidelity. When used alone without STCFG (V2 vs.V3), it improves fidelity at a slight cost to perceptual quality. However, when combined with STCFG (V4 vs.V6), SRCA yields improvements across all four metrics, underscoring its importance and complementary role within the full framework.

Spatially Targeted CFG application (STCFG). STCFG provides a direct mechanism for enhancing ungrounded regions and significantly improves all four metrics, whether used alone (V2 vs.V6), in combination with SRCA (V3 vs.V4), or in combination with both SRCA and different semantic segmentation methods (V9 vs.V7 and V10 vs.V8), demonstrating its effectiveness and versatility.

DAPE vs. Semantic Segmentation. As mentioned in Sec. 3.3, a contemporary work uses semantic segmentation (SS), specifically, Mask2Former [5] pre-trained on ADE20K, to extract semantic labels with complete image coverage. Motivated by their interesting work, we also experimented with

Table 2: Ablation study evaluating the contribution of each component within SRSR. SRCA denotes *spatially re-focused cross-attention*, and STCFG denotes *spatially targeted classifier-free guidance*. Mask2Former and DINO-X represent different semantic segmentation backbones. **Bold** indicates the best performance. Refer to Tab. S1 for the extended ablation results with no-reference metrics.

Version	PSNR↑	SSIM↑	LPIPS↓	DISTS↓
V1: SeeSR	25.1717	0.7219	0.3008	0.2223
V2: SeeSR + Grounding	25.1751	0.7234	0.3001	0.2229
V3: SeeSR + Grounding + SRCA	25.2688	0.7280	0.3013	0.2254
V4: SeeSR + Grounding + SRCA + STCFG (Ours)	26.3996	0.7632	0.2718	0.2092
V5: SeeSR + Grounding + SRCA + STCFG + Ungrounded Tags	26.3871	0.7625	0.2729	0.2095
V6: SeeSR + Grounding + STCFG	26.3986	0.7627	0.2735	0.2112
V7: SeeSR + Grounding + SRCA + STCFG + Mask2Former	26.3128	0.7620	0.2725	0.2093
V8: SeeSR + Grounding + SRCA + STCFG + DINO-X	26.3449	0.7627	0.2722	0.2089
V9: SeeSR + Grounding + SRCA + Mask2Former	26.2885	0.7609	0.2734	0.2098
V10: SeeSR + Grounding + SRCA + DINO-X	26.3221	0.7621	0.2729	0.2090

augmenting the well-performing DAPE tags using SS. However, as shown by comparing V4 and V7 in Tab. 2, performance declined, primarily because SS models, not trained with degradation in design, often produce inaccurate labels. Moreover, Mask2Former recognizes only 150 categories, limiting coverage for real-world SR tasks. This further reduce the semantic accuracy of the extracted texts.

To mitigate these constraints, we tried Prompt-Free Anything Detection and Segmentation in DINO-X [34] (V8 in Tab. 2), which supports open-vocabulary SS. Although it outperforms Mask2Former (V7), it still trails behind using only DAPE (V4). These results reaffirm that inaccurate tags prove more detrimental than incomplete ones - an insight that also reinforces our grounding design.

4.4 Hyper-parameter analysis

The confidence threshold for grounding affects the balance between tag accuracy and coverage. A higher threshold discards less certain tags to boost accuracy, but also reduces coverage. As shown in Table 3, larger thresholds generally yield higher PSNR and SSIM, whereas thresholds of 0.25-0.35 achieve more favorable LPIPS and DISTIS. Overall, SRSR remains robust against varying thresholds: in all cases, it significantly outperforms the baseline in all four metrics. We adopt a confidence threshold of 0.25 for all reported comparisons.

Table 3: Hyper-parameter analysis: different grounding thresholds produce consistent results that outperform the SeeSR baseline on RealSR dataset. **Red** = best, **Blue** = second-best.

Threshold	PSNR \uparrow	SSIM \uparrow	LPIPS \downarrow	DISTS \downarrow
Baseline	25.1717	0.7219	0.3008	0.2223
0.15	26.3632	0.7625	0.2727	0.2093
0.25	26.3996	0.7632	0.2718	0.2092
0.35	26.4550	0.7644	0.2715	0.2099
0.45	26.5378	0.7657	0.2731	0.2112
0.55	26.6008	0.7665	0.2735	0.2124

5 Conclusion

We introduced a *spatially re-focused super-resolution (SRSR)* framework to improve the semantic accuracy of text-conditioned, diffusion-based SR. By grounding and filtering extracted tags, we remove irrelevant text prompts and pair each valid tag with a corresponding segmentation mask. This enables *spatially re-focused cross-attention (SRCA)*, which directs guidance to target regions, and *spatially targeted classifier-free guidance (STCFG)*, which preserves visual fidelity in ungrounded areas. Our approach operates entirely at inference time and can be applied to any cross-attention-based SR model that leverages text priors. Experiments on both synthetic and real-world datasets show that SRSR outperforms seven state-of-the-art methods in fidelity and perceptual quality metrics.

6 Limitations and future works

While SRSR achieves strong gains in both fidelity and semantic accuracy, several limitations and future directions remain. *First*, further exploration of robust, degradation-aware segmentation models could reduce incomplete tag coverage and enhance tagging accuracy. Indeed, our ablation studies that compare Mask2Former with DINO-X suggest that stronger semantic segmentation (SS) backbones improve SRSR’s performance, indicating that future innovations in SS can further enhance our method. *Second*, SRSR is currently designed as an inference-time framework to ensure plug-and-play compatibility with various pre-trained super-resolution models. Although this design enables broad applicability without retraining, incorporating SRSR into the training or fine-tuning process represents an exciting future direction. Doing so would allow the model to internalize the spatial and semantic constraints imposed by SRSR, potentially improving region-specific supervision and semantic localization. However, this integration would come at the cost of additional training complexity and resource demands. *Third*, SRSR’s modular nature allows flexible integration with other Real-ISR frameworks. In this work, we demonstrated its generality through consistent improvements when applied to SeeSR [54] and OSEDiff [53]. Future research could further validate this generality by extending SRSR to broader architectures such as AddSR [56] and TSD-SR [10]. *Finally*, existing no-reference quality metrics remain unreliable, as they often over-reward artifact-heavy or hallucinated outputs (see Fig. 4 and Figures S1–S11). Hence, we emphasize full-reference fidelity and perceptual quality metrics as more trustworthy indicators of restoration faithfulness, which is critical in practical scenarios (e.g., e-commerce product imaging) where visual accuracy directly impacts trust and usability. Nevertheless, when high-quality references are unavailable, the dependence on current no-reference metrics becomes problematic. Developing hallucination-aware no-reference metrics that better align with full-reference measures and human perception is an urgent research need. Promising directions include leveraging vision-language models for perceptual assessment and incorporating penalties for semantic hallucinations.

References

- [1] Eirikur Agustsson and Radu Timofte. NTIRE 2017 Challenge on Single Image Super-Resolution: Dataset and Study. In *Proceedings of the IEEE Conference on Computer Vision and Pattern Recognition Workshops*, pages 126–135, 2017.
- [2] Jianrui Cai, Hui Zeng, Hongwei Yong, Zisheng Cao, and Lei Zhang. Toward real-world single image super-resolution: A new benchmark and a new model. In *Proceedings of the IEEE/CVF International Conference on Computer Vision*, pages 3086–3095, 2019.
- [3] Hanting Chen, Yunhe Wang, Tianyu Guo, Chang Xu, Yiping Deng, Zhenhua Liu, Siwei Ma, Chunjing Xu, Chao Xu, and Wen Gao. Pre-trained image processing transformer. In *Proceedings of the IEEE/CVF Conference on Computer Vision and Pattern Recognition*, pages 12299–12310, 2021.
- [4] Xiangyu Chen, Xintao Wang, Jiantao Zhou, Yu Qiao, and Chao Dong. Activating more pixels in image super-resolution transformer. In *Proceedings of the IEEE/CVF Conference on Computer Vision and Pattern Recognition*, pages 22367–22377, 2023.
- [5] Bowen Cheng, Ishan Misra, Alexander G. Schwing, Alexander Kirillov, and Rohit Girdhar. Masked-attention mask transformer for universal image segmentation. 2022.
- [6] Tao Dai, Jianrui Cai, Yongbing Zhang, Shu-Tao Xia, and Lei Zhang. Second-order attention network for single image super-resolution. In *Proceedings of the IEEE/CVF conference on computer vision and pattern recognition*, pages 11065–11074, 2019.
- [7] Keyan Ding, Kede Ma, Shiqi Wang, and Eero P. Simoncelli. Image quality assessment: Unifying structure and texture similarity. *IEEE Transactions on Pattern Analysis and Machine Intelligence*, 44(5):2567–2581, 2020.
- [8] Chao Dong, Chen Change Loy, Kaiming He, and Xiaoou Tang. Learning a deep convolutional network for image super-resolution. In *Computer Vision—ECCV 2014: 13th European Conference, Zurich, Switzerland, September 6–12, 2014, Proceedings, Part IV*, pages 184–199. Springer, 2014.
- [9] Chao Dong, Chen Change Loy, Kaiming He, and Xiaoou Tang. Image super-resolution using deep convolutional networks. *IEEE Transactions on Pattern Analysis and Machine Intelligence*, 2015.
- [10] Linwei Dong, Qingnan Fan, Yihong Guo, Zhonghao Wang, Qi Zhang, Jinwei Chen, Yawei Luo, and Changqing Zou. Tsd-sr: One-step diffusion with target score distillation for real-world image super-resolution. In *Proceedings of the IEEE/CVF Conference on Computer Vision and Pattern Recognition (CVPR)*, 2025.
- [11] Ian Goodfellow, Jean Pouget-Abadie, Mehdi Mirza, Bing Xu, David Warde-Farley, Sherjil Ozair, Aaron Courville, and Yoshua Bengio. Generative adversarial nets. In Z. Ghahramani, M. Welling, C. Cortes, N. Lawrence, and K.Q. Weinberger, editors, *Advances in Neural Information Processing Systems*, volume 27. Curran Associates, Inc., 2014.
- [12] Hayit Greenspan. Super-resolution in medical imaging. *The Computer Journal*, 52(1):43–63, 02 2008.
- [13] Muhammad Haris, Gregory Shakhnarovich, and Norimichi Ukita. Deep back-projection networks for super-resolution. In *Proceedings of the IEEE conference on computer vision and pattern recognition*, pages 1664–1673, 2018.
- [14] Kaiming He, Xiangyu Zhang, Shaoqing Ren, and Jian Sun. Deep residual learning for image recognition. In *Proceedings of the IEEE Conference on Computer Vision and Pattern Recognition*, pages 770–778, 2016.
- [15] Martin Heusel, Hubert Ramsauer, Thomas Unterthiner, Bernhard Nessler, and Sepp Hochreiter. GANs trained by a two time-scale update rule converge to a local nash equilibrium. In *Advances in Neural Information Processing Systems*, volume 30, 2017.

- [16] Jonathan Ho, Ajay Jain, and Pieter Abbeel. Denoising diffusion probabilistic models. *arXiv preprint arxiv:2006.11239*, 2020.
- [17] Yawen Huang, Ling Shao, and Alejandro F. Frangi. Simultaneous super-resolution and cross-modality synthesis of 3d medical images using weakly-supervised joint convolutional sparse coding. In *Proceedings of the IEEE/CVF conference on computer vision and pattern recognition*, pages 6070–6079, 2017.
- [18] Andrey Ignatov, Radu Timofte, Maurizio Denna, Abdel Younes, Ganzorig Gankhuyag, Jingang Huh, Myeong Kyun Kim, Kihwan Yoon, Hyeon-Cheol Moon, and et al. Efficient and accurate quantized image super-resolution on mobile npus, mobile ai & aim 2022 challenge: Report. In Leonid Karlinsky, Tomer Michaeli, and Ko Nishino, editors, *Computer Vision – ECCV 2022 Workshops*, pages 92–129, Cham, 2023. Springer Nature Switzerland.
- [19] Bahjat Kawar, Michael Elad, Stefano Ermon, and Jiaming Song. Denoising diffusion restoration models. In *Advances in Neural Information Processing Systems*, volume 35, pages 23593–23606, 2022.
- [20] Junjie Ke, Qifei Wang, Yilin Wang, Peyman Milanfar, and Feng Yang. MUSIQ: Multi-scale image quality transformer. In *Proceedings of the IEEE/CVF International Conference on Computer Vision*, pages 5148–5157, 2021.
- [21] Jiwon Kim, Jung Kwon Lee, and Kyoung Mu Lee. Accurate image super-resolution using very deep convolutional networks. In *Proceedings of the IEEE conference on computer vision and pattern recognition*, pages 1646–1654, 2016.
- [22] B Li, X Li, H Zhu, Y Jin, R Feng, Z Zhang, and Z Chen. Sed: Semantic-aware discriminator for image super-resolution. arxiv 2024. *arXiv preprint arXiv:2402.19387*.
- [23] Junnan Li, Dongxu Li, Caiming Xiong, and Steven Hoi. BLIP: Bootstrapping language-image pre-training for unified vision-language understanding and generation. *arXiv preprint arXiv:2201.12086*, 2022.
- [24] Jingyun Liang, Jiezhang Cao, Guolei Sun, Kai Zhang, Luc Van Gool, and Radu Timofte. SwinIR: Image restoration using swin transformer. In *Proceedings of the IEEE/CVF International Conference on Computer Vision*, pages 1833–1844, 2021.
- [25] Xinqi Lin, Jingwen He, Ziyang Chen, Zhaoyang Lyu, Ben Fei, Bo Dai, Wanli Ouyang, Yu Qiao, and Chao Dong. Diffbir: Towards blind image restoration with generative diffusion prior. *arXiv preprint arXiv:2308.15070*, 2023.
- [26] Haotian Liu, Chunyuan Li, Qingyang Wu, and Yong Jae Lee. Visual instruction tuning. In *Advances in Neural Information Processing Systems*, volume 36, 2024.
- [27] Chenxi Ma. Uncertainty-aware gan for single image super resolution. In *Proceedings of the AAAI Conference on Artificial Intelligence*, volume 38, pages 4071–4079, 2024.
- [28] Jianqi Ma, Shi Guo, and Lei Zhang. Text prior guided scene text image super-resolution. *IEEE Transactions on Image Processing*, 32:1341–1353, 2023.
- [29] Alexander Quinn Nichol and Prafulla Dhariwal. Improved denoising diffusion probabilistic models. In *ICML*, volume 139 of *Proceedings of Machine Learning Research*, pages 8162–8171. PMLR, 2021.
- [30] JoonKyu Park, Sanghyun Son, and Kyoung Mu Lee. Content-aware local gan for photo-realistic super-resolution. In *Proceedings of the IEEE/CVF International Conference on Computer Vision*, pages 10585–10594, 2023.
- [31] Yunpeng Qu, Kun Yuan, Kai Zhao, Qizhi Xie, Jinhua Hao, Ming Sun, and Chao Zhou. Xpsr: Cross-modal priors for diffusion-based image super-resolution. *arXiv preprint arXiv:2403.05049*, 2024.

- [32] Pejman Rasti, Tõnis Uiboupin, Sergio Escalera, and Gholamreza Anbarjafari. Convolutional neural network super resolution for face recognition in surveillance monitoring. In Francisco José Perales and Josef Kittler, editors, *Articulated Motion and Deformable Objects*, pages 175–184, Cham, 2016. Springer International Publishing.
- [33] Joseph Redmon, Santosh Divvala, Ross Girshick, and Ali Farhadi. You only look once: Unified, real-time object detection. In *Proceedings of the IEEE Conference on Computer Vision and Pattern Recognition*, pages 779–788, 2016.
- [34] Tianhe Ren, Yihao Chen, Qing Jiang, Zhaoyang Zeng, Yuda Xiong, Wenlong Liu, Zhengyu Ma, Junyi Shen, Yuan Gao, Xiaoke Jiang, Xingyu Chen, Zhuheng Song, Yuhong Zhang, Hongjie Huang, Han Gao, Shilong Liu, Hao Zhang, Feng Li, Kent Yu, and Lei Zhang. Dino-x: A unified vision model for open-world object detection and understanding, 2024.
- [35] Tianhe Ren, Shilong Liu, Ailing Zeng, Jing Lin, Kunchang Li, He Cao, Jiayu Chen, Xinyu Huang, Yukang Chen, Feng Yan, Zhaoyang Zeng, Hao Zhang, Feng Li, Jie Yang, Hongyang Li, Qing Jiang, and Lei Zhang. Grounded sam: Assembling open-world models for diverse visual tasks, 2024.
- [36] Robin Rombach, Andreas Blattmann, Dominik Lorenz, Patrick Esser, and Björn Ommer. High-resolution image synthesis with latent diffusion models. In *Proceedings of the IEEE/CVF Conference on Computer Vision and Pattern Recognition*, pages 10684–10695, 2022.
- [37] Haoze Sun, Wenbo Li, Jianzhuang Liu, Haoyu Chen, Renjing Pei, Xueyi Zou, Youliang Yan, and Yujiu Yang. Coser: Bridging image and language for cognitive super-resolution. In *Proceedings of the IEEE/CVF Conference on Computer Vision and Pattern Recognition (CVPR)*, 2024.
- [38] Lingchen Sun, Jie Liang, Shuaizheng Liu, Hongwei Yong, and Lei Zhang. Perception-distortion balanced super-resolution: A multi-objective optimization perspective. *arXiv preprint arXiv:2312.15408*, 2023.
- [39] Chunwei Tian, Yong Xu, Wangmeng Zuo, Bob Zhang, Lunke Fei, and Chia-Wen Lin. Coarse-to-fine cnn for image super-resolution. *IEEE Transactions on Multimedia*, 23:1489–1502, 2020.
- [40] Li-Yuan Tsao, Hao-Wei Chen, Hao-Wei Chung, Deqing Sun, Chun-Yi Lee, Kelvin C. K. Chan, and Ming-Hsuan Yang. Holisdip: Image super-resolution via holistic semantics and diffusion prior. *arXiv preprint arXiv:2411.18662*, 2024.
- [41] Sabina Umirzakova, Shabir Ahmad, Latif U. Khan, and Taegkeun Whangbo. Medical image super-resolution for smart healthcare applications: A comprehensive survey. *Information Fusion*, 103:102075, 2024.
- [42] Uddeshya Upadhyay, Viswanath P Sudarshan, and Suyash P Awate. Uncertainty-aware gan with adaptive loss for robust mri image enhancement. In *Proceedings of the IEEE/CVF International Conference on Computer Vision*, pages 3255–3264, 2021.
- [43] Jianyi Wang, Kelvin CK Chan, and Chen Change Loy. Exploring clip for assessing the look and feel of images. In *Proceedings of the AAAI Conference on Artificial Intelligence*, volume 37, pages 2555–2563, 2023.
- [44] Jianyi Wang, Zongsheng Yue, Shangchen Zhou, Kelvin CK Chan, and Chen Change Loy. Exploiting diffusion prior for real-world image super-resolution. *International Journal of Computer Vision*, pages 1–21, 2024.
- [45] Peijuan Wang, Bulent Bayram, and Elif Sertel. A comprehensive review on deep learning based remote sensing image super-resolution methods. *Earth-Science Reviews*, 232:104110, 2022.
- [46] Xintao Wang, Liangbin Xie, Chao Dong, and Ying Shan. Real-ESRGAN: Training real-world blind super-resolution with pure synthetic data. In *Proceedings of the IEEE/CVF International Conference on Computer Vision*, pages 1905–1914, 2021.

- [47] Xintao Wang, Ke Yu, Chao Dong, and Chen Change Loy. Recovering realistic texture in image super-resolution by deep spatial feature transform. In *Proceedings of the IEEE Conference on Computer Vision and Pattern Recognition (CVPR)*, 2018.
- [48] Yan Wang, Yi Liu, Shijie Zhao, Junlin Li, and Li Zhang. Camixersr: Only details need more" attention". In *Proceedings of the IEEE/CVF Conference on Computer Vision and Pattern Recognition*, pages 25837–25846, 2024.
- [49] Yinhuai Wang, Jiwen Yu, and Jian Zhang. Zero-shot image restoration using denoising diffusion null-space model. *arXiv preprint arXiv:2212.00490*, 2022.
- [50] Yufei Wang, Wenhan Yang, Xinyuan Chen, Yaohui Wang, Lanqing Guo, Lap-Pui Chau, Ziwei Liu, Yu Qiao, Alex C Kot, and Bihan Wen. SinSR: Diffusion-based image super-resolution in a single step. *arXiv preprint arXiv:2311.14760*, 2023.
- [51] Zhou Wang, Alan C. Bovik, Hamid R. Sheikh, and Eero P. Simoncelli. Image quality assessment: From error visibility to structural similarity. *IEEE Transactions on Image Processing*, 13(4):600–612, 2004.
- [52] Pengxu Wei, Ziwei Xie, Hannan Lu, Zongyuan Zhan, Qixiang Ye, Wangmeng Zuo, and Liang Lin. Component divide-and-conquer for real-world image super-resolution. In *Computer Vision—ECCV 2020: 16th European Conference, Glasgow, UK, August 23–28, 2020, Proceedings, Part VIII*, pages 101–117. Springer, 2020.
- [53] Rongyuan Wu, Lingchen Sun, Zhiyuan Ma, and Lei Zhang. One-step effective diffusion network for real-world image super-resolution. *arXiv preprint arXiv:2406.08177*, 2024.
- [54] Rongyuan Wu, Tao Yang, Lingchen Sun, Zhengqiang Zhang, Shuai Li, and Lei Zhang. Seesr: Towards semantics-aware real-world image super-resolution. In *Proceedings of the IEEE/CVF conference on computer vision and pattern recognition*, pages 25456–25467, 2024.
- [55] Jiahua Xiao, Jiawei Zhang, Dongqing Zou, Xiaodan Zhang, Jimmy Ren, and Xing Wei. Semantic segmentation prior for diffusion-based real-world super-resolution. *arXiv preprint arXiv:2412.02960*, 2024.
- [56] Rui Xie, Chen Zhao, Kai Zhang, Zhenyu Zhang, Jun Zhou, Jian Yang, and Ying Tai. Addr: Accelerating diffusion-based blind super-resolution with adversarial diffusion distillation. *arXiv preprint arXiv:2404.01717*, 2024.
- [57] Sidi Yang, Tianhe Wu, Shuwei Shi, Shanshan Lao, Yuan Gong, Mingdeng Cao, Jiahao Wang, and Yujiu Yang. MANIQA: Multi-dimension attention network for no-reference image quality assessment. In *Proceedings of the IEEE/CVF Conference on Computer Vision and Pattern Recognition*, pages 1191–1200, 2022.
- [58] Tao Yang, Rongyuan Wu, Peiran Ren, Xuansong Xie, and Lei Zhang. Pixel-aware stable diffusion for realistic image super-resolution and personalized stylization. In *The European Conference on Computer Vision (ECCV)*, 2024.
- [59] Fanghua Yu, Jinjin Gu, Zheyuan Li, Jinfan Hu, Xiangtao Kong, Xintao Wang, Jingwen He, Yu Qiao, and Chao Dong. Scaling up to excellence: Practicing model scaling for photo-realistic image restoration in the wild, 2024.
- [60] Zongsheng Yue, Jianyi Wang, and Chen Change Loy. ResShift: Efficient diffusion model for image super-resolution by residual shifting. *arXiv preprint arXiv:2307.12348*, 2023.
- [61] Hanwen Zhang, Yi Wang, Xiqian Zhang, and Hong Tian. Lsd: Large-window semantic-aware discriminator for image super-resolution reconstruction. In *Proceedings of the 2024 International Conference on Intelligent Perception and Pattern Recognition*, pages 6–12, 2024.
- [62] Kai Zhang, Jingyun Liang, Luc Van Gool, and Radu Timofte. Designing a practical degradation model for deep blind image super-resolution. In *Proceedings of the IEEE/CVF International Conference on Computer Vision*, pages 4791–4800, 2021.

- [63] Liangpei Zhang, Hongyan Zhang, Huanfeng Shen, and Pingxiang Li. A super-resolution reconstruction algorithm for surveillance images. *Signal Processing*, 90(3):848–859, 2010.
- [64] Lin Zhang, Lei Zhang, and Alan C. Bovik. A feature-enriched completely blind image quality evaluator. *IEEE Transactions on Image Processing*, 24(8):2579–2591, 2015.
- [65] Lvmin Zhang, Anyi Rao, and Maneesh Agrawala. Adding conditional control to text-to-image diffusion models, 2023.
- [66] Richard Zhang, Phillip Isola, Alexei A Efros, Eli Shechtman, and Oliver Wang. The unreasonable effectiveness of deep features as a perceptual metric. In *Proceedings of the IEEE Conference on Computer Vision and Pattern Recognition*, pages 586–595, 2018.
- [67] Xindong Zhang, Hui Zeng, Shi Guo, and Lei Zhang. Efficient long-range attention network for image super-resolution. In *European Conference on Computer Vision*, pages 649–667. Springer, 2022.
- [68] Youcai Zhang, Xinyu Huang, Jinyu Ma, Zhaoyang Li, Zhaochuan Luo, Yanchun Xie, Yuzhuo Qin, Tong Luo, Yaqian Li, Shilong Liu, et al. Recognize anything: A strong image tagging model. *arXiv preprint arXiv:2306.03514*, 2023.
- [69] Yulun Zhang, Yapeng Tian, Yu Kong, Bineng Zhong, and Yun Fu. Residual dense network for image super-resolution. In *Proceedings of the IEEE conference on computer vision and pattern recognition*, pages 2472–2481, 2018.
- [70] Bolei Zhou, Hang Zhao, Xavier Puig, Sanja Fidler, Adela Barriuso, and Antonio Torralba. Scene parsing through ade20k dataset. In *Proceedings of the IEEE Conference on Computer Vision and Pattern Recognition (CVPR)*, pages 633–641, 2017.

Supplementary Material

Outline of supplementary material. This supplementary material provides additional results, analyses, and discussions to support the main paper. It is structured as follows:

- In Section A, we present extensive qualitative comparisons and visual analyses by comparing the baseline results and cross-attention maps before and after integrating our proposed SRSR framework. These examples demonstrate the effectiveness and internal mechanisms of the SRCA and STCFG components within the SRSR framework (Figures S1–S11).
- Section B extends this analysis to an ablation variant that uses semantic segmentation masks for prompt extraction. This supplements the quantitative ablation study results in Section 4.3 of the main paper and supports the claim in Section 3.3 that semantic segmentation has two key limitations (lack of degradation awareness and constrained vocabulary size), which lead to inferior results compared to our approach based on DAPE and Grounded SAM (Figures S12–S15).
- In Section C, we provide additional qualitative comparisons paired with quantitative metrics to highlight a key observation: no-reference metrics often misjudge and favor hallucinated outputs (Figures S16–S17).
- Section D presents an additional user study evaluating human perceptual preferences between the baseline results and those produced after integrating SRSR (Figure S18). The study shows that human annotators consistently prefer our SRSR-enhanced outputs.
- Section E supplements the ablation results in Tab.2 with no-reference metrics (Tab. S1), further showing that while full-reference fidelity and perceptual metrics align with visual quality improvements, existing no-reference metrics often produce misleading trends and over-reward artifact-heavy outputs.
- Finally, Section F provides a clarification on potential societal impacts.

All figure references include detailed captions to support discussion and analysis of the corresponding findings.

A Additional qualitative comparisons and visual analysis

As a plug-and-play module, the effectiveness of SRSR is most clearly demonstrated by comparing the performance of the same baseline before and after integration. In this section, we present additional qualitative comparisons and visual analyses (Figures S1–S11) to support the following key takeaways:

1. **Enhanced semantic fidelity.** We provide [qualitative comparisons](#) that highlight the ability of SRSR to improve semantic fidelity by removing hallucinations. *While baseline results may appear visually appealing, they often contain hallucinated objects or textures that are semantically inconsistent with the ground-truth high-resolution image.* In contrast, our method produces restorations that better align with the true image content.
2. **Limitations of no-reference metrics.** Alongside visual results, we include [corresponding quantitative comparisons](#). We emphasize that *no-reference metrics, which lack access to the ground-truth high-resolution image, tend to misjudge and often reward hallucinated outputs.* This is evident in the performance drop of these metrics when hallucinations are removed. Conversely, full-reference metrics (PSNR and SSIM for fidelity, and LPIPS and DISTS for perceptual quality) provide a more reliable assessment of semantic and visual accuracy. SRSR demonstrates superior performance in these full-reference evaluations.
3. **Visual analysis of SRCA and STCFG effects.** To further illustrate the mechanisms of our proposed components, we include [auxiliary visualizations](#) such as the re-focused versus original cross-attention maps or the ungrounded region masks. These demonstrate how *SRCA enhances text-token alignment with relevant regions* and how *STCFG effectively suppresses text influence in ungrounded areas to prevent hallucinations.*

All figures presented in this section are accompanied by detailed captions to support discussion and analysis of the corresponding findings.

B Comparing prompt extraction methods: DAPE vs. Semantic Segmentation

As discussed in Section 3.3 of the main paper, we also experimented with using semantic segmentation to extract grounded tag–region pairs, and compared its performance with our final method that employs DAPE and Grounded SAM for the same goal. We observed two key limitations when using semantic segmentation compared to DAPE: *First*, unlike DAPE, which is trained to be degradation-aware when extracting tags from low-quality LR images, standard semantic segmentation models lack this capability and tend to extract incorrect tags more frequently, leading to restoring hallucinated contents that are not faithful to the ground-truth HR image. *Second*, Semantic segmentation models often have a limited vocabulary size, which restricts their expressiveness and precision in practice. This leads to the extraction of coarse prompts that result in imprecise or incorrect restorations. These issues result in inferior performance compared to our final approach, which uses DAPE for prompt extraction followed by Grounded SAM for visual grounding.

As reported in Section 4.3 of the main paper, we already presented ablation studies with quantitative comparisons. In this section, we supplement those results with additional qualitative comparisons and analysis. Specifically, the figures correspond to supporting the following key takeaways:

1. **Semantic segmentation models lack degradation awareness.** Figures S12–S13 highlight that this limitation *causes incorrect prompts to be confidently extracted*, which then misguide the restoration process and lead to semantically incorrect outputs.
2. **Semantic segmentation models have constrained vocabulary size.** Figures S14–S15 illustrate that this limitation *reduces the expressiveness and precision of prompt extraction*. As a result, using only coarsely related prompts to guide the restoration process leads to suboptimal outcomes.
3. **Limitations of no-reference metrics.** Same as in Section A, all figures in this section (Figures S12–S15) further demonstrate the drawbacks of no-reference metrics: *they frequently misjudge and favor outputs that contain hallucinations resulting from incorrect text conditioning*, demonstrating their limitations in assessing semantic fidelity for super-resolution.

All figures presented in this section are also accompanied by detailed captions to support discussion and analysis of the corresponding findings.

C More qualitative comparisons illustrating no-reference metrics’ limitations

The previous two sections have already highlighted the limitations of no-reference metrics by comparing our method against both the baseline and an ablation variant that uses semantic segmentation masks for prompt extraction. In this section (Figures S16–S17), we provide additional visual comparisons (paired with corresponding quantitative metrics) between our method and other baseline approaches to further underscore the shortcomings of no-reference metrics.

D Additional user study results

We have also conducted a user study to evaluate human perceptual preferences between the baseline results before and after integrating our SRSR framework. Given the size of the synthetic DIV2K dataset, we focus the study on two real-world datasets: RealSR and DRealSR, using their entire datasets. For each image, we presented the low-resolution input along with two anonymized high-resolution outputs (ours: SRSR-SeeSR and the baseline: SeeSR) labeled ‘Method A’ and ‘Method B’. Two annotators were asked to select the preferred image or indicate if both appeared visually similar, with evaluations based on sharpness, visual realism, and detail preservation. The order of presentation was randomized, and full images were shown (not crops) to avoid bias. Results are aggregated and visualized in bar charts (Figure S18), showing that SRSR-SeeSR is consistently preferred over the baseline SeeSR across both datasets.

Table S1: Ablation study evaluating the contribution of each component within SRSR. SRCA denotes *spatially re-focused cross-attention*, STCFG denotes *spatially targeted classifier-free guidance*, and G refers to grounding. Mask2Former and DINO-X represent different semantic segmentation backbones. **Bold** indicates the best performance.

Version	PSNR \uparrow	SSIM \uparrow	LPIPS \downarrow	DISTS \downarrow	FID \downarrow	NIQE \downarrow	MUSIQ \uparrow	MANIQA \uparrow	CLIPQA \uparrow
V1: SeeSR	25.1717	0.7219	0.3008	0.2223	125.55	5.4081	69.77	0.6442	0.6612
V2: SeeSR + G	25.1751	0.7234	0.3001	0.2229	128.41	5.4852	69.84	0.6436	0.6701
V3: SeeSR + G + SRCA	25.2688	0.7280	0.3013	0.2254	132.55	5.5029	69.91	0.6422	0.6683
V4: SeeSR + G + SRCA + STCFG (Ours)	26.3996	0.7632	0.2718	0.2092	126.31	5.8627	62.88	0.5628	0.5409
V5: V4 + Ungrounded Tags	26.3871	0.7625	0.2729	0.2095	126.28	5.8657	63.15	0.5665	0.5460
V6: SeeSR + G + STCFG	26.3986	0.7627	0.2735	0.2112	127.24	5.8947	62.99	0.5648	0.5456
V7: SeeSR + G + SRCA + STCFG + Mask2Former	26.3128	0.7620	0.2725	0.2093	127.51	5.8026	63.31	0.5689	0.5477
V8: SeeSR + G + SRCA + STCFG + DINO-X	26.3449	0.7627	0.2722	0.2089	127.77	5.8196	63.17	0.5670	0.5450
V9: SeeSR + G + SRCA + Mask2Former	26.2885	0.7609	0.2734	0.2098	127.19	5.7801	63.73	0.5728	0.5543
V10: SeeSR + G + SRCA + DINO-X	26.3221	0.7621	0.2729	0.2090	127.33	5.7927	63.58	0.5713	0.5520

E Extended ablation results

To further strengthen our point that the existing no-reference metrics are flawed that they tend to over-reward artifact-heavy or hallucinated outputs, in Tab. S1, we supplement the no-reference metrics to the ablation results in Tab. 2.

Tab. S1 highlights a consistent trend: improvements in full-reference fidelity metrics (PSNR, SSIM) and perceptual quality metrics (LPIPS, DISTS) align with observed improvements in visual and semantic fidelity, as supported by our qualitative analysis (e.g., Fig. 4 and Figures S1–S11). However, the same changes often lead to worse results in all no-reference metrics (NIQE, MUSIQ, MANIQA, CLIPQA), which can misleadingly favor outputs with hallucinated or artifact-heavy details. For example, removing STCFG (V3) from our full version (V4) improves all no-reference metrics, even though fidelity, full-reference perceptual quality, and visual quality drop. Similarly, removing SRCA (V6) worsens both fidelity and full-reference perceptual quality, yet again, no-reference metrics do not consistently reflect this decline. This pattern also holds when comparing DINO-X to Mask2Former (V8/V7, V10/V9): fidelity, full-reference perceptual quality metrics, and visual quality are better with DINO-X, which aligns with the inherent advantages of DINO-X over Mask2Former, as we elaborated in Sec. 4.3. However, no-reference metrics show the reverse trend. These findings reinforce our point that current no-reference metrics often fail to penalize hallucinations and can mislead practical evaluation, especially in Real-ISR.

F Clarification on potential negative societal impact

Our work focuses on enhancing the visual quality of low-resolution images through super-resolution techniques with improved semantic fidelity. It is primarily intended for applications in image restoration, photography, and scientific imaging, where enhancing degraded real-world content is valuable. Our method does not involve any user or personally identifiable information, and our evaluation is conducted on public, non-sensitive datasets. Therefore, we believe our work does not pose significant societal risks. On the contrary, it may benefit the aforementioned intended applications where detail-preserving enhancement is crucial.

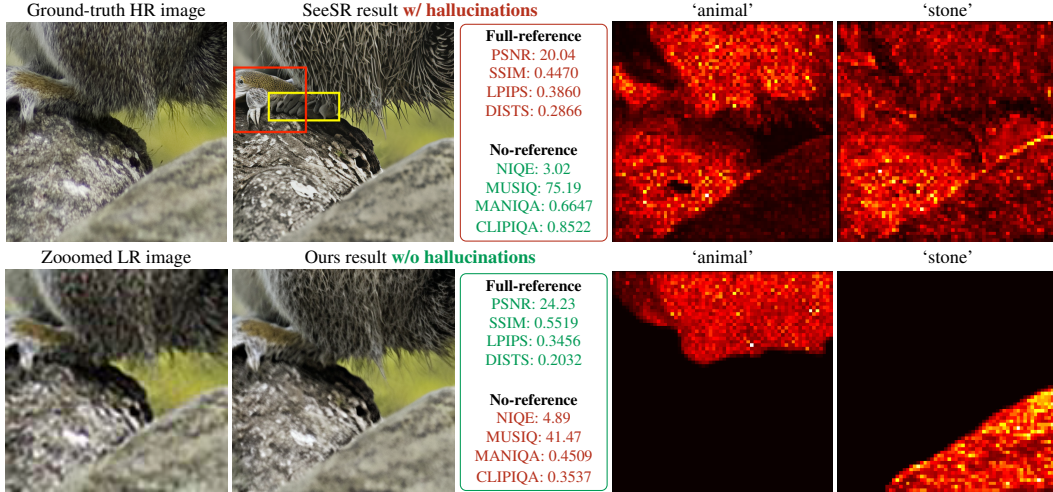


Figure S1: Column 1: Paired LR-HR images. Column 2: Qualitative comparisons of the baseline with and without our proposed SRSR. Column 3: Corresponding quantitative metrics. Columns 4–5: Attention visualizations for selected tokens to illustrate the effect of SRSR. In the region highlighted by the red bounding box, the object is actually an animal’s claw, but it is difficult to recognize in the degraded LR image. Consequently, the prompt extractor (DAPE) fails to extract relevant tags such as ‘claw’. As a result, the baseline model attributes this region to the token ‘animal’ according to the cross-attention map, and hallucinates it as a vivid fish. Similarly, in the yellow bounding box, the region corresponds to the animal’s fur, but is misinterpreted due to degradation. The baseline instead applies influence from the unrelated tag ‘stone’, resulting in a texture resembling small pebbles. Beyond these highlighted objects, the baseline also introduces other over-synthesized textures in the ‘animal’ and ‘stone’ regions that deviate from the ground-truth HR image, despite being visually plausible. In contrast, our SRSR framework assigns tags only to regions where grounding confidence is high (e.g., ‘animal’, ‘stone’), leaving uncertain regions, such as the red region, ungrounded. Within the SRSR framework, SRCA ensures that grounded regions are not influenced by irrelevant tokens, thereby removing hallucinations from the ‘animal’ and ‘stone’ areas. Additionally, STCFG applies unconditional predictions to ungrounded regions like the animal’s claw, suppressing inappropriate text influence while preserving perceptual quality.

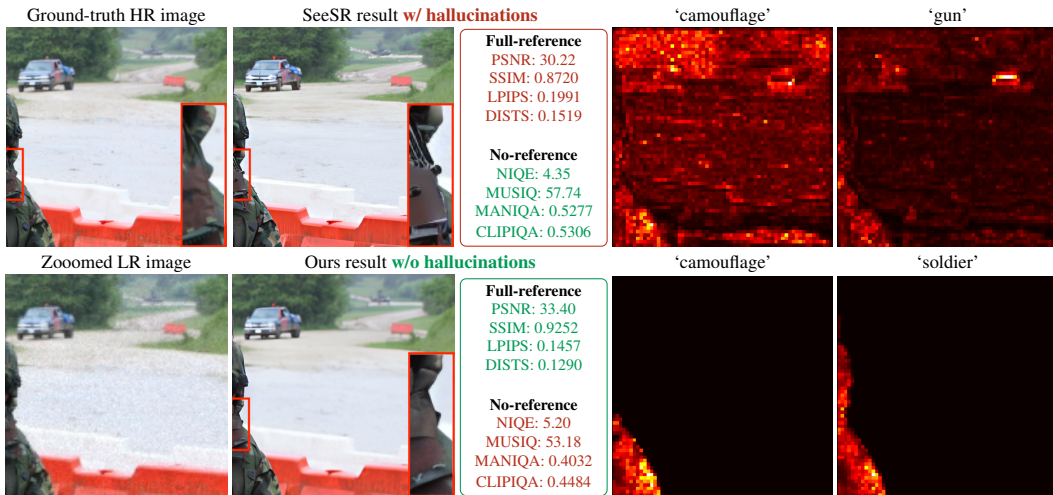


Figure S2: Column 1: Paired LR-HR images. Column 2: Qualitative comparisons of the baseline with and without our proposed SRSR. Column 3: Corresponding quantitative metrics. Columns 4–5: Attention visualizations for selected tokens to illustrate the effect of SRSR. In the highlighted region, the baseline hallucinates gun-like objects due to incorrect tags like ‘gun’ and ‘rifle’ extracted by DAPE, which misattribute attention to parts of the ‘camouflage’ object. In contrast, our SRSR framework removes such irrelevant tags via grounding and re-focuses attention on salient concepts like ‘camouflage’ and ‘soldier’, resulting in semantically faithful restorations.

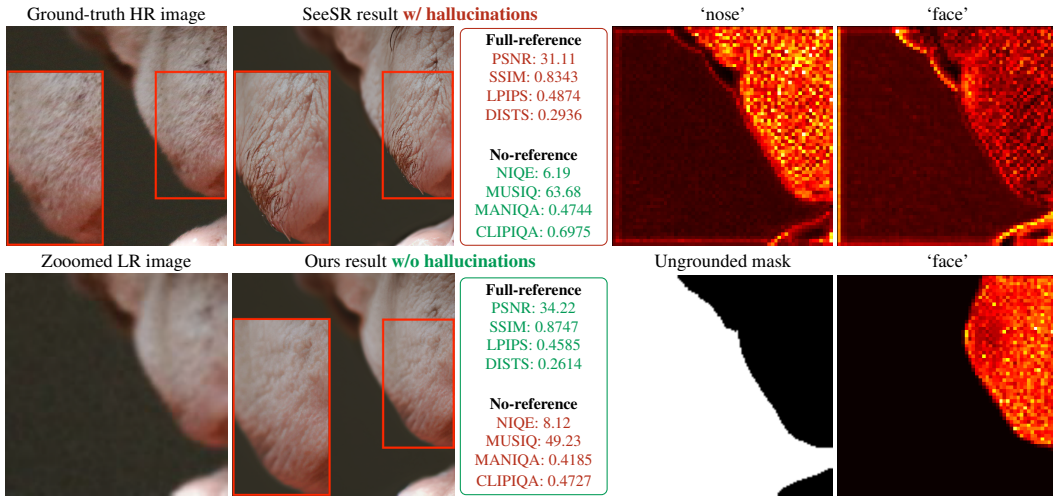


Figure S3: Column 1: Paired LR-HR images. Column 2: Qualitative comparisons of the baseline with and without our proposed SRSR. Column 3: Corresponding quantitative metrics. Columns 4-5: Ungrounded region mask and attention visualizations for selected tokens to illustrate the effect of SRSR. In the highlighted region, the baseline hallucinates nose hairs on the face due to incorrect tags like ‘nose’ and ‘mouth’ extracted by DAPE, which misattribute attention to parts of the ‘face’ object. In contrast, our SRSR framework removes such irrelevant tags via grounding and re-focuses attention on salient concepts like ‘face’, resulting in semantically faithful restorations.

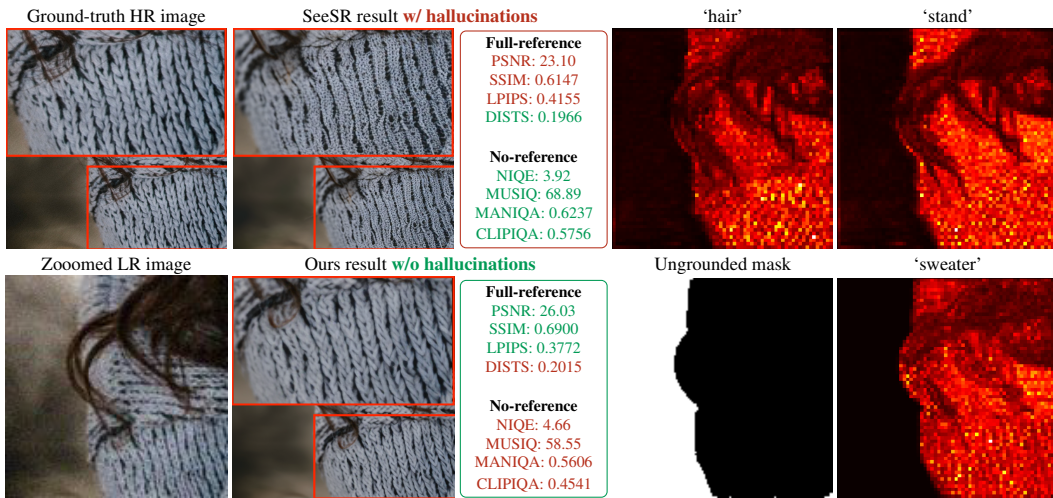


Figure S4: Column 1: Paired LR-HR images. Column 2: Qualitative comparisons of the baseline with and without our proposed SRSR. Column 3: Corresponding quantitative metrics. Columns 4-5: Ungrounded region mask and attention visualizations for selected tokens to illustrate the effect of SRSR. In the highlighted region, the baseline produces sweater textures that deviate from the ground-truth HR image, influenced by unrelated tags such as ‘hair’ and incorrect tags like ‘stand’, as indicated by the cross-attention maps. In contrast, our SRSR framework employs SRCA to eliminate irrelevant tag influence and localize text conditioning strictly to grounded regions, associating the sweater region only with the tag ‘sweater’, thereby ensuring more faithful and semantically accurate restorations.

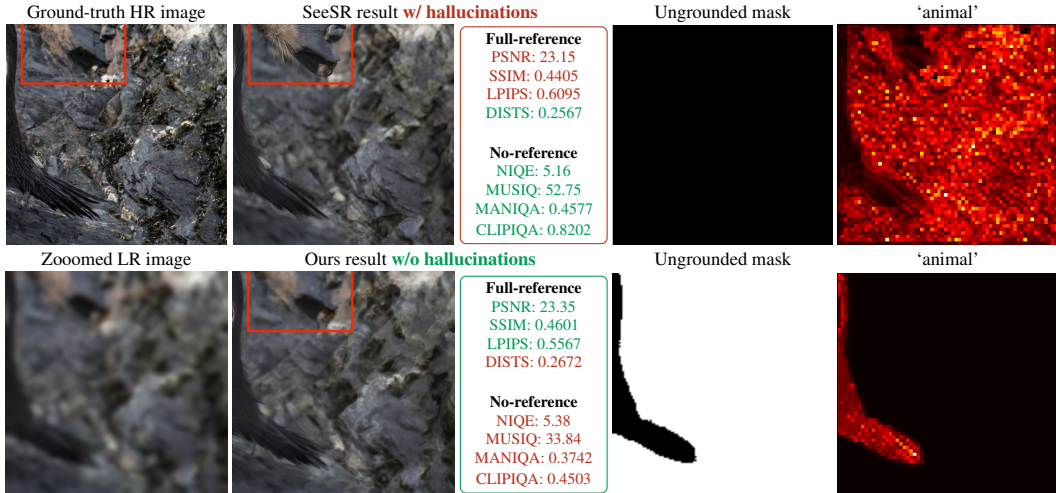


Figure S5: Column 1: Paired LR-HR images. Column 2: Qualitative comparisons of the baseline with and without our proposed SRSR. Column 3: Corresponding quantitative metrics. Columns 4-5: Ungrounded region mask and attention visualizations for selected tokens to illustrate the effect of SRSR. In the baseline, the inherent cross-attention for the token ‘animal’ is broadly dispersed across the image, including the highlighted region corresponding to the stone object, leading to hallucinated animal-like features in that area (note the stone is mistakenly restored with fur-like textures). Our SRSR framework addresses this by first applying SRCA to constrain the token ‘animal’ to its grounded region, correcting misaligned attention. However, ungrounded regions remain susceptible to influence from global tokens such as EOS, padding, and punctuation, which can introduce noise and semantic summary of the entire prompt. To address this, we introduce STCFG to explicitly avoid applying text conditioning to ungrounded regions, resulting in more semantically faithful restorations.

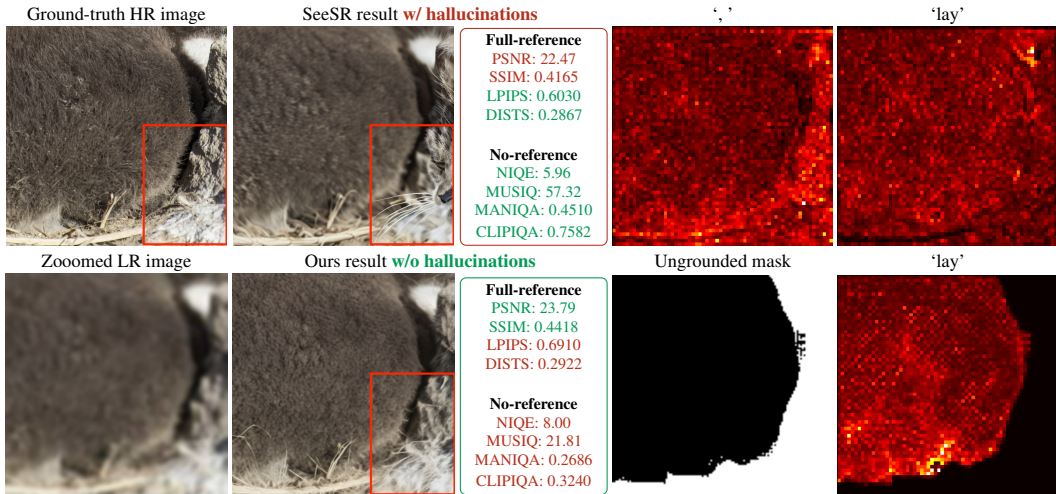


Figure S6: Column 1: Paired LR-HR images. Column 2: Qualitative comparisons of the baseline with and without our proposed SRSR. Column 3: Corresponding quantitative metrics. Columns 4-5: Ungrounded region mask and attention visualizations for selected tokens to illustrate the effect of SRSR. The highlighted region is heavily degraded and should depict stone and weed in the ground-truth HR image. However, the baseline incorrectly restores it as a cat’s face with whiskers, which is visually plausible but semantically inaccurate. The baseline’s cross-attention maps reveal that the punctuation token ‘ , ’ and the irrelevant token ‘lay’ attend to this region. These lack meaningful semantics or relevance to the scene, resulting in hallucinated content during restoration. By contrast, our SRSR framework applies SRCA to constrain the influence of tokens like ‘lay’ to their grounded regions and uses STCFG to apply unconditional generation in ungrounded areas (as identified by the ungrounded mask), effectively suppressing hallucinations and improving semantic fidelity.

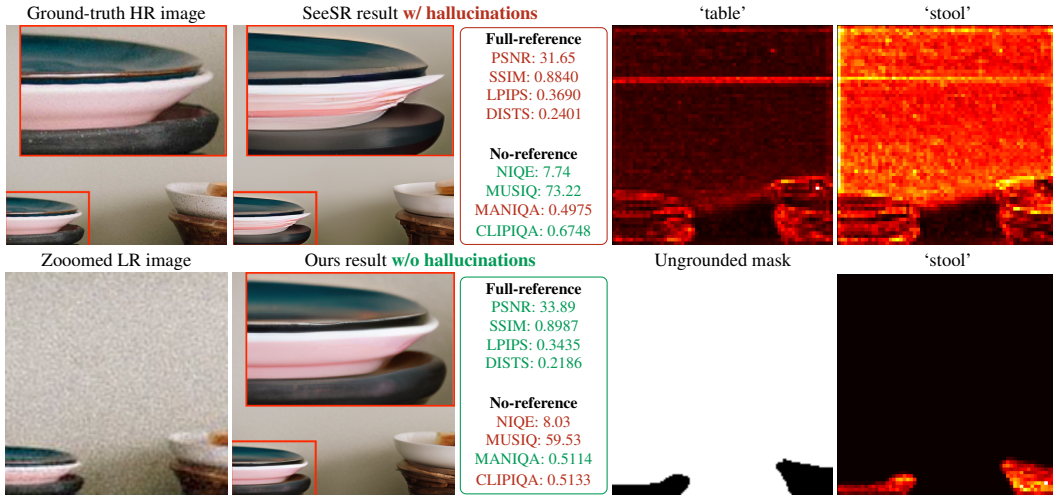


Figure S7: Column 1: Paired LR-HR images. Column 2: Qualitative comparisons of the baseline with and without our proposed SRSR. Column 3: Corresponding quantitative metrics. Columns 4-5: Ungrounded region mask and attention visualizations for selected tokens to illustrate the effect of SRSR. The key objects in this example are two stacks of plates, each placed on a supporting base. While DAPE successfully extracts the semantically related tag ‘stool’ for the base structures, it fails to recognize the plates due to severe degradation in the LR image. In the baseline, the cross-attention for the tag ‘stool’ is diffusely distributed across irrelevant regions, and additional tags such as ‘table’ and ‘stool’ incorrectly attend to the plate areas. This misattribution results in visible artifacts in the restored plates and suboptimal reconstruction of the base. In contrast, our SRSR framework leverages SRCA to re-focus attention on correctly grounded regions (e.g., the base) and uses STCFG to suppress text-based influence in ungrounded regions (e.g., the plates), yielding more accurate and faithful restorations.

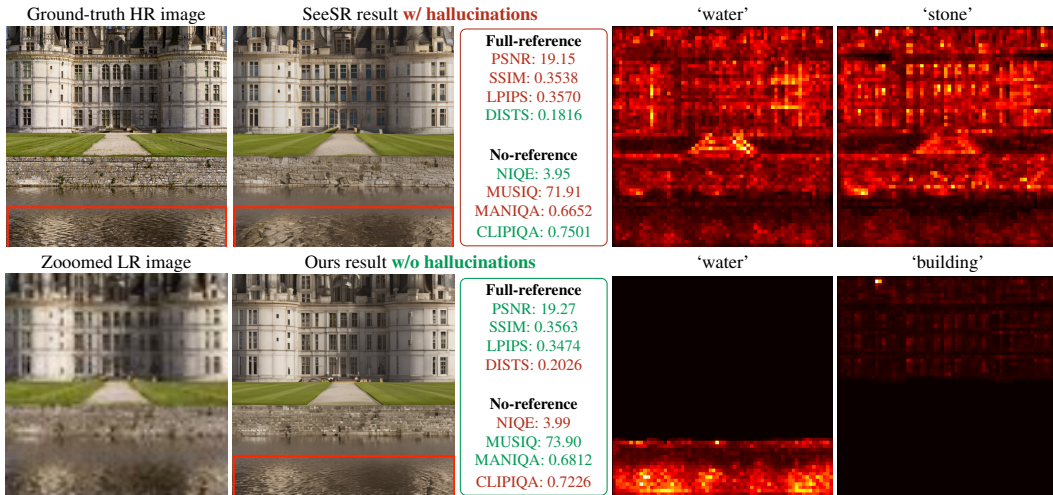


Figure S8: Column 1: Paired LR-HR images. Column 2: Qualitative comparisons of the baseline with and without our proposed SRSR. Column 3: Corresponding quantitative metrics. Columns 4-5: Attention visualizations for selected tokens to illustrate the effect of SRSR. In the highlighted water regions, the baseline introduces unnatural patterns, influenced by the irrelevant token ‘stone’ and the misdirected attention of the relevant token ‘water’ to incorrect spatial areas. By contrast, our SRSR framework leverages SRCA to re-focus each token’s influence within its grounded spatial region, producing semantically more faithful and visually accurate restorations.

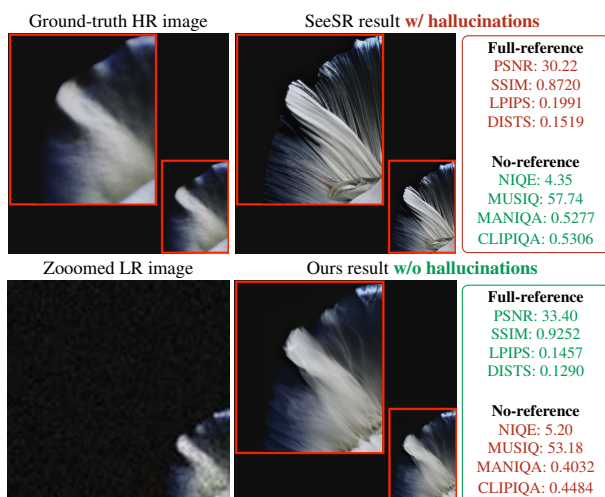


Figure S9: Column 1: Paired LR-HR images. Column 2: Qualitative comparisons of the baseline with and without our proposed SRSR. Column 3: Corresponding quantitative metrics. In this example, DAPE fails to extract any meaningful tags, leaving only global tokens (e.g., SOS, EOS, punctuation) to drive text conditioning. The baseline forces the application of text guidance even in such cases, causing the model to hallucinate textures despite the prompt carrying no semantic value. In contrast, our SRSR framework uses STCFG to disable text conditioning in ungrounded regions (here, the entire image), applying only unconditional prediction during denoising. This suppresses hallucinated details and improves alignment with the ground-truth HR image.

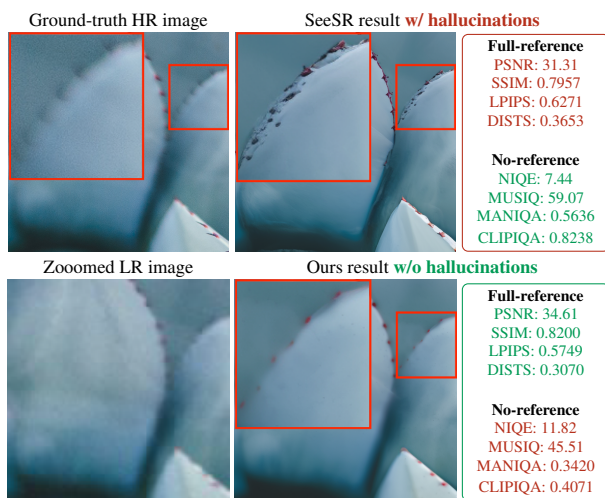


Figure S10: Column 1: Paired LR-HR images. Column 2: Qualitative comparisons of the baseline with and without our proposed SRSR. Column 3: Corresponding quantitative metrics. In this example, DAPE fails to extract any meaningful tags, leaving only global tokens (e.g., SOS, EOS, punctuation) to drive text conditioning. The baseline forces the application of text guidance even in such cases, causing the model to hallucinate textures despite the prompt carrying no semantic value. In contrast, our SRSR framework uses STCFG to disable text conditioning in ungrounded regions (here, the entire image), applying only unconditional prediction during denoising. This suppresses hallucinated details and improves alignment with the ground-truth HR image.

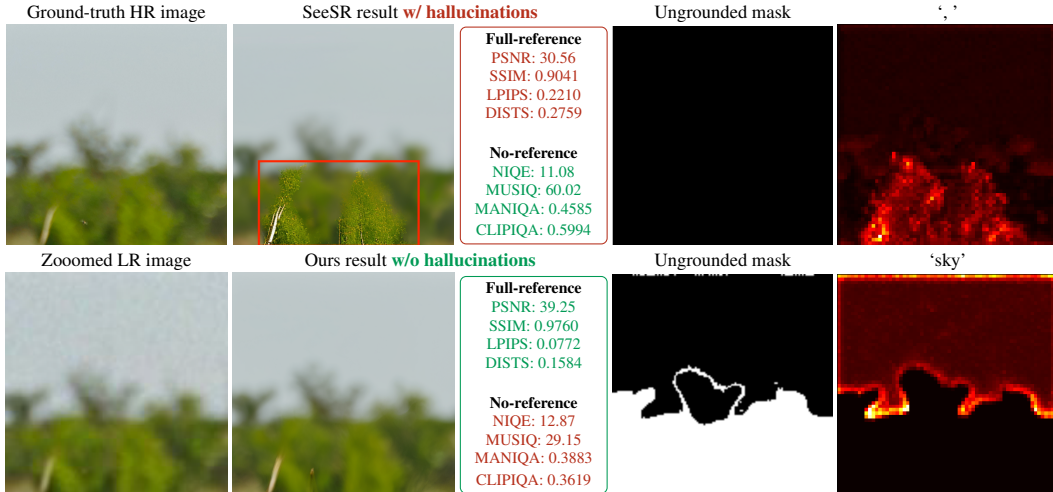


Figure S11: Column 1: Paired LR-HR images. Column 2: Qualitative comparisons of the baseline with and without our proposed SRSR. Column 3: Corresponding quantitative metrics. Columns 4-5: Ungrounded region mask and attention visualizations for selected tokens to illustrate the effect of SRSR. In the baseline, the inherent cross-attention maps show that only the punctuation token ‘,’ attends to the highlighted region. However, this token carries no meaningful semantics, and its influence during the generation process introduces noise and hallucinated details that deviate from the ground-truth HR image. In contrast, our SRSR framework leverages STCFG to apply unconditional generation specifically to regions that cannot be confidently grounded (i.e., those indicated by the ungrounded mask), effectively removing such hallucinations and improving semantic fidelity.

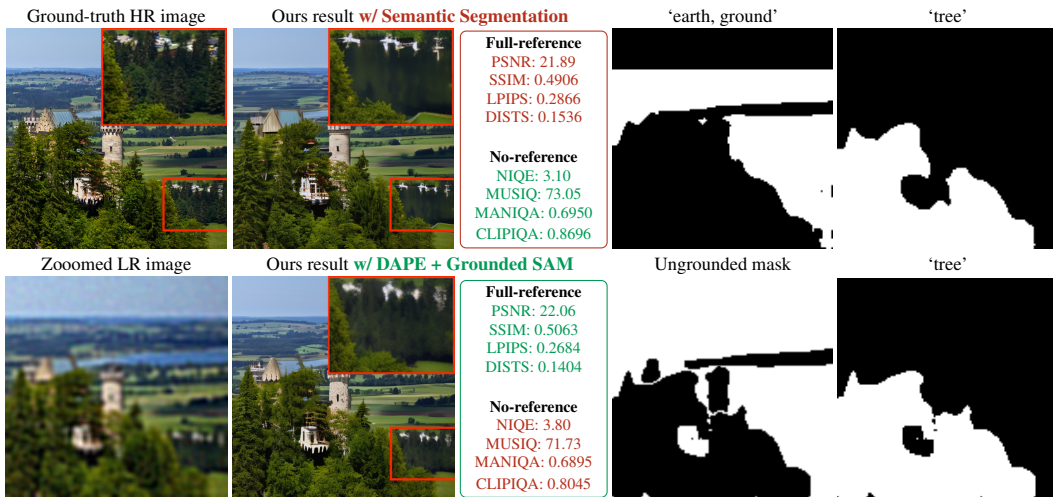


Figure S12: Column 1: Paired LR-HR images. Column 2: Qualitative comparisons of our results using semantic segmentation versus DAPE + Grounded SAM for prompt extraction and grounding. Column 3: Corresponding quantitative metrics. Columns 4–5: Grounded masks for selected tokens, where white indicates grounded regions. Unlike DAPE, which is trained to be degradation-aware when extracting tags from low-quality LR images, standard semantic segmentation models lack this capability and tend to extract incorrect tags more frequently. In the highlighted region, the semantic segmentation model confidently grounds the tag ‘earth, ground’, leading to a ground-like restoration that is inconsistent with the true content (trees) seen in the HR image. In contrast, DAPE is more degradation-aware, thus fails to confidently ground any tag for this region due to the severe degradation, triggering our STCFG mechanism to apply unconditional generation. This results in more faithful tree-like restoration and effectively prevents the introduction of semantically incorrect content.

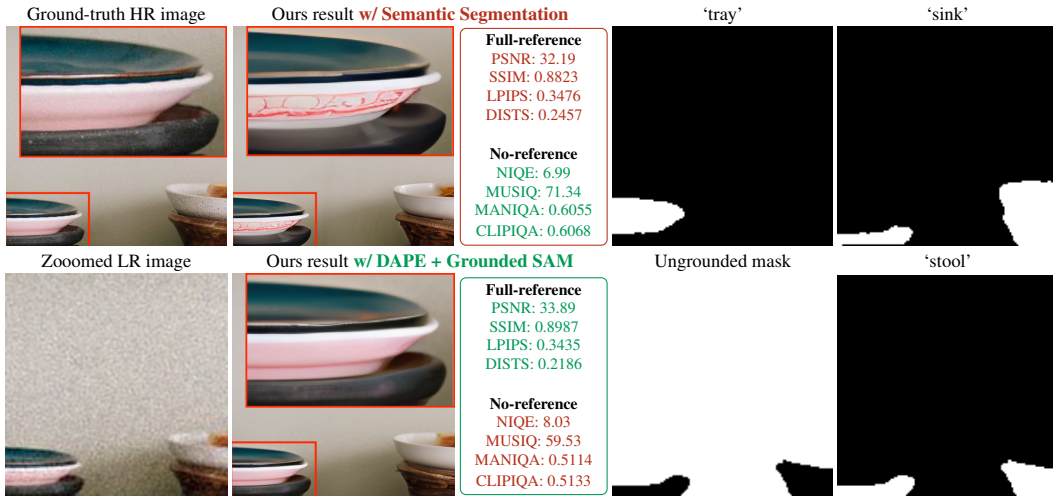


Figure S13: Column 1: Paired LR-HR images. Column 2: Qualitative comparisons of our results using semantic segmentation versus DAPE + Grounded SAM for prompt extraction and grounding. Column 3: Corresponding quantitative metrics. Columns 4–5: Grounded masks for selected tokens, where white indicates grounded regions. Unlike DAPE, which is trained to be degradation-aware when extracting tags from low-quality LR images, standard semantic segmentation models lack this capability and tend to extract incorrect tags more frequently. In the highlighted region, the semantic segmentation model grounds tags such as ‘tray’ and ‘sink’, which leads to hallucinated content — misrepresenting both the plates and the base beneath them. In contrast, DAPE extracts the tag ‘stool’, which more appropriately describes the supporting base. For the severely degraded plate regions, DAPE does not assign any confident tag, triggering our STCFG mechanism to apply unconditional generation. This helps produce more semantically accurate restorations and avoids introducing misleading visual artifacts.

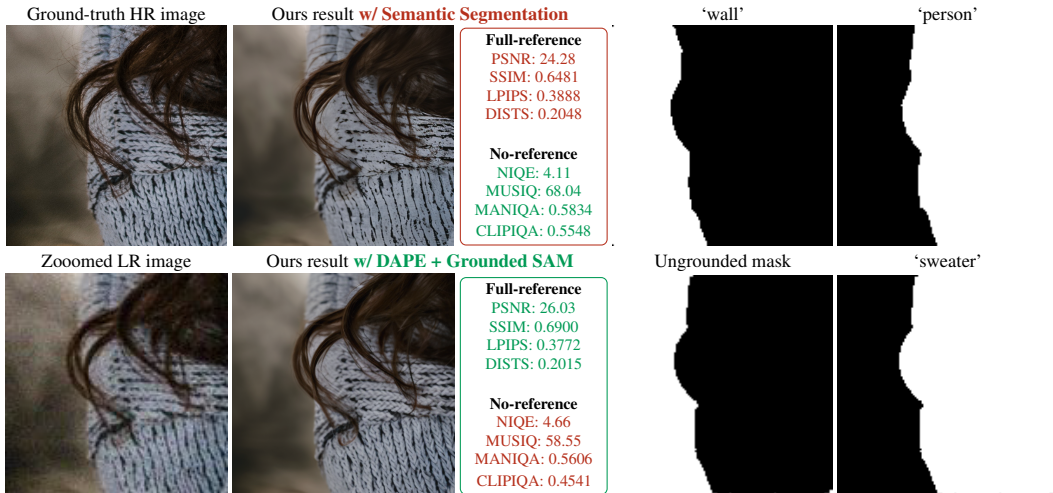


Figure S14: Column 1: Paired LR-HR images. Column 2: Qualitative comparisons of our results using semantic segmentation versus DAPE + Grounded SAM for prompt extraction and grounding. Column 3: Corresponding quantitative metrics. Columns 4–5: Grounded masks for selected tokens, where white indicates grounded regions. Due to the limited vocabulary of semantic segmentation models, the extracted prompt (‘person’) is a coarse descriptor and leads to imprecise restorations of the sweater’s textures. In contrast, our method leverages DAPE with a broader vocabulary and grounds the more appropriate tag ‘sweater’ via Grounded SAM, resulting in semantically faithful restorations.

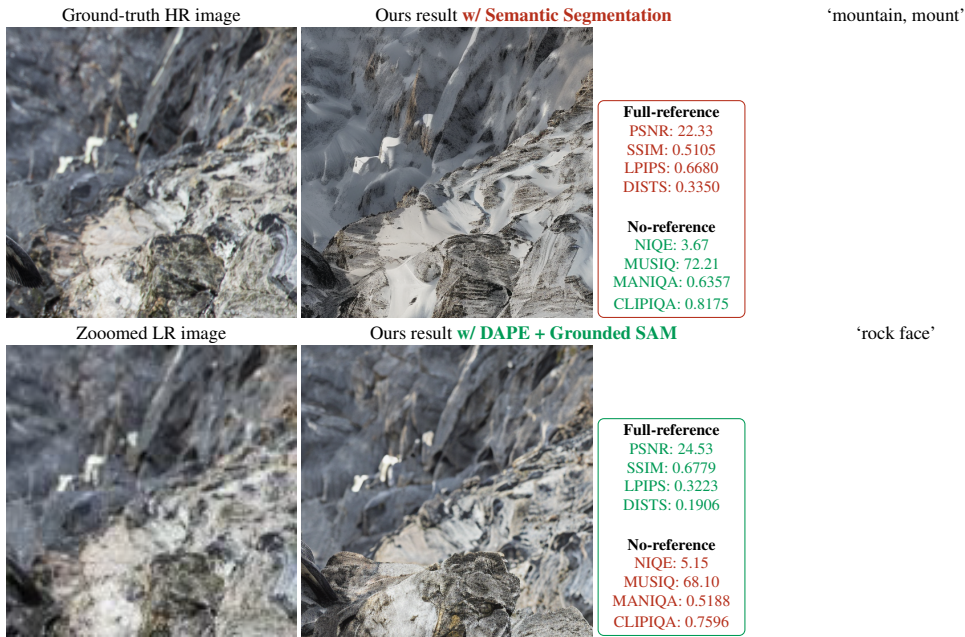


Figure S15: Column 1: Paired LR-HR images. Column 2: Qualitative comparisons of our results using semantic segmentation versus DAPE + Grounded SAM for prompt extraction and grounding. Column 3: Corresponding quantitative metrics. Columns 4: Grounded masks for selected tokens, where white indicates grounded regions. Both approaches ground the entire image with a single tag, as reflected by the fully white masks. However, due to the limited vocabulary of semantic segmentation models, the extracted prompt ('mountain, mount') is a coarse descriptor and leads to mountain-like hallucinations. In contrast, our method leverages DAPE with a broader vocabulary and grounds the more appropriate tag 'rock face' via Grounded SAM, resulting in semantically faithful restorations.

Ground-truth HR image	Baselines result w/ hallucinations		Ours result w/o hallucinations	
		Full-reference PSNR: 27.33 SSIM: 0.9322 LPIPS: 0.1074 DIST: 0.2347 No-reference NIQE: 10.64 MUSIQ: 64.09 MANIQA: 0.5370 CLIPQA: 0.7957		Full-reference PSNR: 30.23 SSIM: 0.9614 LPIPS: 0.1037 DIST: 0.1782 No-reference NIQE: 12.15 MUSIQ: 54.86 MANIQA: 0.4626 CLIPQA: 0.6521
		Full-reference PSNR: 26.03 SSIM: 0.8097 LPIPS: 0.2267 DIST: 0.2040 No-reference NIQE: 5.27 MUSIQ: 74.49 MANIQA: 0.5799 CLIPQA: 0.8527		Full-reference PSNR: 26.23 SSIM: 0.8305 LPIPS: 0.1962 DIST: 0.1946 No-reference NIQE: 7.43 MUSIQ: 73.51 MANIQA: 0.5464 CLIPQA: 0.7485
		Full-reference PSNR: 23.16 SSIM: 0.6000 LPIPS: 0.4855 DIST: 0.1965 No-reference NIQE: 3.10 MUSIQ: 64.20 MANIQA: 0.5249 CLIPQA: 0.7226		Full-reference PSNR: 24.88 SSIM: 0.6681 LPIPS: 0.3534 DIST: 0.1897 No-reference NIQE: 5.02 MUSIQ: 55.41 MANIQA: 0.4274 CLIPQA: 0.6180
		Full-reference PSNR: 23.91 SSIM: 0.6726 LPIPS: 0.3994 DIST: 0.2518 No-reference NIQE: 4.31 MUSIQ: 65.31 MANIQA: 0.5041 CLIPQA: 0.7818		Full-reference PSNR: 27.24 SSIM: 0.7533 LPIPS: 0.2857 DIST: 0.1530 No-reference NIQE: 4.40 MUSIQ: 41.95 MANIQA: 0.3726 CLIPQA: 0.5750
		Full-reference PSNR: 22.58 SSIM: 0.5044 LPIPS: 0.4516 DIST: 0.2321 No-reference NIQE: 2.57 MUSIQ: 72.02 MANIQA: 0.6062 CLIPQA: 0.8033		Full-reference PSNR: 25.42 SSIM: 0.6772 LPIPS: 0.2957 DIST: 0.1565 No-reference NIQE: 5.05 MUSIQ: 66.15 MANIQA: 0.4729 CLIPQA: 0.7932

Figure S16: Additional qualitative results paired with quantitative metrics reveal that *no-reference metrics tend to misjudge and heavily reward hallucinated results*. This exposes their limitations in assessing semantic fidelity in super-resolution tasks.

Ground-truth HR image	Baselines result w/ hallucinations		Ours result w/o hallucinations	
		Full-reference PSNR: 21.80 SSIM: 0.3201 LPIPS: 0.5507 DIST: 0.2599 No-reference NIQE: 3.94 MUSIQ: 52.18 MANIQA: 0.5951 CLIPQA: 0.6970		Full-reference PSNR: 23.22 SSIM: 0.4065 LPIPS: 0.4448 DIST: 0.2160 No-reference NIQE: 5.25 MUSIQ: 48.97 MANIQA: 0.5212 CLIPQA: 0.4137
		Full-reference PSNR: 24.93 SSIM: 0.6983 LPIPS: 0.3464 DIST: 0.1729 No-reference NIQE: 5.33 MUSIQ: 58.68 MANIQA: 0.5179 CLIPQA: 0.7575		Full-reference PSNR: 25.78 SSIM: 0.7436 LPIPS: 0.3318 DIST: 0.1716 No-reference NIQE: 6.37 MUSIQ: 42.89 MANIQA: 0.4494 CLIPQA: 0.4323
		Full-reference PSNR: 28.17 SSIM: 0.7751 LPIPS: 0.2136 DIST: 0.2191 No-reference NIQE: 5.93 MUSIQ: 69.54 MANIQA: 0.5680 CLIPQA: 0.5731		Full-reference PSNR: 31.84 SSIM: 0.8470 LPIPS: 0.1871 DIST: 0.1370 No-reference NIQE: 6.22 MUSIQ: 59.87 MANIQA: 0.5041 CLIPQA: 0.4901
		Full-reference PSNR: 23.64 SSIM: 0.3591 LPIPS: 0.9140 DIST: 0.3978 No-reference NIQE: 3.50 MUSIQ: 65.77 MANIQA: 0.6918 CLIPQA: 0.6129		Full-reference PSNR: 32.80 SSIM: 0.9037 LPIPS: 0.4783 DIST: 0.3909 No-reference NIQE: 7.75 MUSIQ: 25.29 MANIQA: 0.2965 CLIPQA: 0.2303
		Full-reference PSNR: 21.58 SSIM: 0.3667 LPIPS: 0.4973 DIST: 0.2100 No-reference NIQE: 2.25 MUSIQ: 70.02 MANIQA: 0.6558 CLIPQA: 0.8059		Full-reference PSNR: 22.76 SSIM: 0.4137 LPIPS: 0.4152 DIST: 0.1938 No-reference NIQE: 3.48 MUSIQ: 57.73 MANIQA: 0.6182 CLIPQA: 0.5514

Figure S17: Additional qualitative results paired with quantitative metrics reveal that *no-reference metrics tend to misjudge and heavily reward hallucinated results*. This exposes their limitations in assessing semantic fidelity in super-resolution tasks.

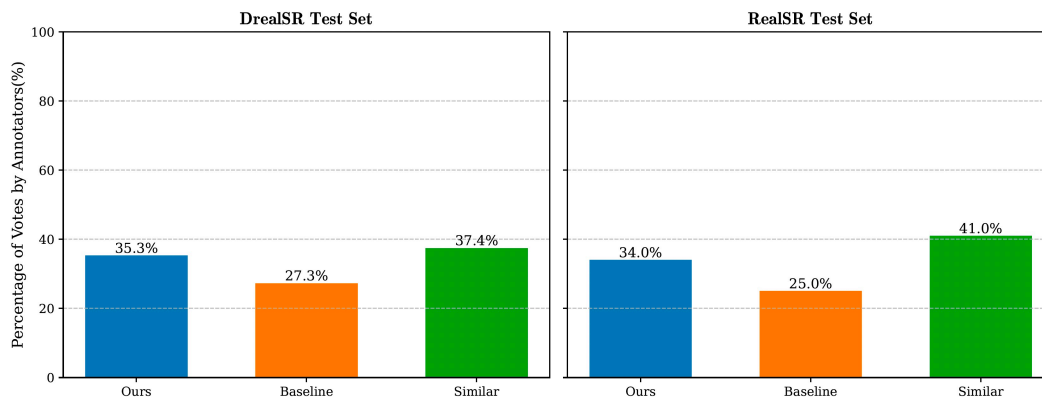


Figure S18: User study results evaluating human perceptual preferences between the baseline results and those produced after integrating SRSR. The study shows that human annotators consistently prefer our SRSR-enhanced outputs.